nature portfolio

Peer Review File

Synergistic versatile bistriflimide salts in light-accelerated spiro-OMeTAD oxidation and perovskite module photovoltaics engineering

Corresponding Author: Professor Yabing Qi

This file contains all reviewer reports in order by version, followed by all author rebuttals in order by version.

Version 0:

Reviewer comments:

Reviewer #1

(Remarks to the Author)
The paper titled “Light-initiated oxidation of spiro-OMeTAD by versatile bistriflimide salts in efficient and stable perovskite solar modules” by Jiahao Zhang was inspired by the commonly known phenomenon of the self-oxidation of the Spiro-OMeTAD under illumination. The authors systematically examine the underlying doping mechanism and leverage it to design new additives that enable efficient and stable perovskite solar modules, achieving certified high performance. Here are some of my comments for this work:
1. For the paragraph from line 200 – 219, it is interesting to see that THF can reduce the amount of the usage of tBP. But there are some problems. (1) The authors demonstrate that THF enables the reduction of tBP concentration without damaging the perovskite film. However, it remains unclear whether the addition of THF or the reduction in tBP affects the p-doping level of the spiro-OMeTAD film. Additional clarification or supporting data would be helpful here. (2) Try to make the optimization of THF: tBP ratio as a standard paragraph. This will make paper much clearer to read. The rest of the original paragraph could be moved to ‘The LODT doping mechanism with LiTFSI and its replacement by NH4TFSI’ part.
2. From line 331-341, this paragraph illustrates the process of strengthening perovskite film by ATFSI (PEA or OA). I can see the discussion about OA and its GIXRD in Figure S22. But the discussion about PEA and Figure S23 and Figure S24 are in SI. Could the author move it to the main text? This would be helpful for readers to understand the story of the choice of large cation between OA and PEA.
3. The manuscript focuses on the light-oxidation doping treatment (LODT) applied to spiro-OMeTAD in solution. Have the authors observed similar doping effects when LODT is applied directly to spiro-OMeTAD films? Furthermore, is it feasible to fabricate complete devices and then apply the LODT method post-fabrication to achieve comparable device performance? Clarification on this point would be valuable for understanding the practical applicability of the method.
4. Can the authors provide time-resolved PL (TRPL), or space-charge limited current (SCLC) measurements of the perovskite films with and without KTFSI? These data would be very helpful for elucidating the impact of KTFSI on the optoelectronic properties and trap-state passivation of the perovskite layer.
5. It would further enrich the manuscript if the authors could compare the charge transfer dynamics between the traditional doping strategy and the LODT approach. For instance, TRPL or transient absorption (TA) spectroscopy on perovskite/HTL stacks could provide insight into the interfacial carrier dynamics and efficiency of hole extraction in both scenarios.
6. When discussing dopants for spiro-OMeTAD, the authors are encouraged to engage more thoroughly with recent literature to acknowledge key developments in the field. In particular, we recommend that the authors review and cite the following significant contributions, which offer a comprehensive overview of progress and insights into molecular doping strategies:
https://doi.org/10.1016/j.mser.2024.100875 (2025)
https://pubs.rsc.org/en/content/articlehtml/2021/ee/d1ee02095a (2021)
https://pubs.rsc.org/en/content/articlelanding/2021/ta/d0ta11564a (2020)
https://pubs.rsc.org/en/content/articlehtml/2019/sc/c8sc05284k (2019)

Reviewer #2

(Remarks to the Author)

In this work, Zhang et al. developed a light-induced doping strategy for Spiro-OMeTAD that eliminated the need for post-oxidation by triggering the spontaneous generation of protons in the Spiro-OMeTAD solution. This approach also enabled the construction of Li-free Spiro-OMeTAD-based perovskite solar cells by replacing LiTFSI with a series of synthesized ammonium TFSI salts. Additionally, they introduced TFSI salts into perovskite films, which promoted the growth of larger grains with fewer surface defects. Through synergistic regulation of both the HTL and perovskite layers using TFSI salts, they achieved highly efficient and stable perovskite solar cells. While the use of ammonium TFSI salts to dope Spiro-OMeTAD is novel, the light-induced doping method has been widely reported (e.g., Joule 2024, 8, 1707; Nature 2021, 594, 51). Thus, the authors should clearly highlight the advantages of their proposed strategy compared to these pioneering studies. Further technical comments are provided below.
In light of these concerns, I recommend that the authors address the critical issues and make the necessary revisions before the manuscript can be considered for further evaluation.

1.It seems that the authors employ tBP as an additive for doping Spiro-OMeTAD via the LODT strategy. However, several critical details require clarification:
(1)Was tBP added during the LODT Spiro-HT solution preparation, or only afterward?
(2)If tBP was omitted, could CB/THF alone dissolve the synthesized ammoniumTFSI?
(3)Is tBP merely a processing aid (solubilizer) or does it actively participate in doping?
2.If the authors used tBP as an additive for doping Spiro-OMeTAD through their LODT strategy. To properly evaluate this work's contribution, the manuscript should clearly compare this approach with established doping methods from previous studies (DOI: 10.1126/science.abo2757; DOI: 10.1038/s41467-024-52199-4; DOI: 10.1002/anie.202316183).
3.The authors claimed “the higher XRD intensity indicated improved crystallinity” in Line 282, which seems to be not inaccurate. XRD intensity depends on multiple factors including instrumental parameters.
4.The retarding effect of TFSI on the FAI-PbI2 reaction kinetics, and its consequent impact on grain growth, requires further mechanistic clarification. Could the authors discuss potential chemical interactions or phase evolution data supporting this observation?
5.The doped Spiro-OMeTAD exhibits a relatively low glass transition temperature, which limits the thermal stability of perovskite solar cells. The authors should conduct relevant stability assessments and include a dedicated discussion on this aspect.
6.In line 341, the authors claimed “Furthermore, we found that OATFSI could also be employed in our LODT method by co-mixing with NH4TFSI.”, it seems that no more details were provided for confirm this point.
7.Given that the spiro-OMeTAD HTL was deposited via spin-coating—a technique with limited scalability—have the authors explored scalable deposition methods (e.g., blade-coating or slot-die coating) to validate the generalizability of their proposed mechanism for industrial-scale fabrication? Such validation would strengthen the practical relevance of this work.
8.The absence of aperture masks during mini-module certification raises concerns about potential overestimation of performance metrics. Moreover, the observed PCE discrepancy between forward/reverse scans suggests significant hysteresis—a behavior inconsistent with the significantly reduced hysteresis characteristics reported for small-area devices.

Reviewer #3

(Remarks to the Author)
Zhang et al. reports a lithium-free and air-free oxidation of spiro-OMeTAD using a combination of organic ammonium TFSI salts and UV light. In addition to spiro-OMeTAD oxidation, other TFSI salts are also investigated for 3D perovskite doping and interface passivation: (1) potassium TFSI is added to the 3D perovskite to improve crystallisation and grain size, and (2) octylammonium TFSI is used to form a 2D/3D perovskite passivation layer. The authors then fabricated small area and mini-module solar cells with improved efficiency. However, lithium-free oxidation, air-free oxidation, and UV-assisted oxidation of spiro-OMeTAD have all been reported many times before. For example doi.org/10.1126/science.abo2757, doi.org/10.1002/aenm.201901519, doi.org/10.1038/s41467-024-52199-4, 10.1016/j.joule.2024.03.012, doi.org/10.1021/acsaem.4c01314. The use of potassium and octylammonium salts are also very common in the literature. This manuscript presents no new insights that have not been reported before in previous literature. In addition, the solar cell results here are not competitive with current standards in the literature, especially compared to the inverted pin devices that are efficient and stable even at high temperatures (85°C). This reviewer also has further technical concerns regarding the authors’ claims below.

(1) UV light above the bandgap of spiro (>3.2eV) is required for photo-oxidisation. Yet, the authors claim that ambient light can trigger spiro photo-oxidisation. Since ambient light (LED or fluorescent) does not emit UV, so what is the UV source? The authors should provide a spectrum of their ambient light. In addition, how does the optical power and emission spectrum of UV affect the LODT spiro oxidation?

(2) Related to above, 10 ppm O2/H2O is 2 orders magnitude higher than a standard glovebox (<0.1ppm). In this case, have the authors excluded O2/H2O contamination in the glovebox assisting with the spiro oxidation?

(3) What is the role of tBP and THF in the LODT spiro? tBP-free and lithium-free spiro has already been demonstrated for pre-oxidised spiro (e.g. doi.org/10.1126/science.abo2757), so is tBP and THF still necessary? The experiments in Fig. S7 may not be relevant because tBP is diluted in the solvent (e.g. chlorobenzene) during spiro deposition on to the perovskite.

(4) Most of the characterizations are done on single-component NH4TFSI spiro. But then the authors switched to using a

dual-component OATFSI and NH4TFSI spiro to fabricate the devices. Does OATFSI change the spiro properties? If so, the characterizations results (e.g. oxidation process, band alignment shifts, conductivity, XPS) are not accurate anymore.

Reviewer #4

(Remarks to the Author)
I co-reviewed this manuscript with one of the reviewers who provided the listed reports. This is part of the Nature Communications initiative to facilitate training in peer review and to provide appropriate recognition for Early Career Researchers who co-review manuscripts.

Version 1:

Reviewer comments:

Reviewer #1

(Remarks to the Author)
The authors have made substantial improvements to the manuscript and addressed all of my concerns. I am happy to recommend this article for publication in Nature Communications.

Reviewer #2

(Remarks to the Author)
The authors have conducted extensive experiments to refine the LODT mechanism and have adequately addressed my concerns. I recommend the manuscript for publication in its current form.

Reviewer #3

(Remarks to the Author)
The authors have improved the quality of their manuscript. My concerns regarding the oxidation mechanism and role of components in LODT spiro have been addressed by the authors. Thus, I can now recommend publication of this work.

Reviewer #4

(Remarks to the Author)
I co-reviewed this manuscript with one of the reviewers who provided the listed reports. This is part of the Nature Communications initiative to facilitate training in peer review and to provide appropriate recognition for Early Career Researchers who co-review manuscripts.

Response to Reviewer #1

The paper titled "Light-initiated oxidation of spiro-OMeTAD by versatile bistriflimide salts in efficient and stable perovskite solar modules" by Jiahao Zhang was inspired by the commonly known phenomenon of the self-oxidation of the Spiro-OMeTAD under illumination. The authors systematically examine the underlying doping mechanism and leverage it to design new additives that enable efficient and stable perovskite solar modules, achieving certified high performance. Here are some of my comments for this work:

Reply:

Thank you for the valuable comments and suggestions, which help us further improve our manuscript. We have carefully read them. Below please find our point-by-point responses. For your convenience, the major changes we have made in the manuscript and the SI are highlighted in yellow.

1#1. For the paragraph from line 200 – 219, it is interesting to see that THF can reduce the amount of the usage of tBP. But there are some problems. (1) The authors demonstrate that THF enables the reduction of tBP concentration without damaging the perovskite film. However, it remains unclear whether the addition of THF or the reduction in tBP affects the p-doping level of the spiro-OMeTAD film. Additional clarification or supporting data would be helpful here. (2) Try to make the optimization of THF: tBP ratio as a standard paragraph. This will make paper much clearer to read. The rest of the original paragraph could be moved to 'The LODT doping mechanism with LiTFSI and its replacement by NH4TFSI' part.

***Reply1*:**

Thank you for your comments. To address your concerns, we conducted the relevant experiment and revised related paragraphs.

(1) As discussed on Page 8, lines 183-194 in "**Incorporation of THF with *t*BP in LODT-HTL**", here, we supplemented additional experiments probing the energy-level shifts for different *t*BP/THF ratios (**Fig. 3b**). Through the UPS data, we found that spiro-HTL treated with LODT showed lower WF and HOMO values without any *t*BP. However, upon increasing the concentration of *t*BP, we observed a complex trade-off evaluating the electronic properties, doping efficiency, thermal stability, and conductivity of LODT-HTL films. For example, regarding electronic properties, with the addition of a small amount of *t*BP (*t*BP/THF ratio of 0.67), both the WF and the HOMO level shifted to deeper energy levels compared to the *t*BP-free film. However, upon further increasing the *t*BP concentration, the Fermi level shifted significantly upward and away from the HOMO level. This increasing energy gap between the HOMO and Fermi levels is a clear indication that *t*BP has a de-doping effect on the oxidized spiro-HTL **Fig. 3b**.

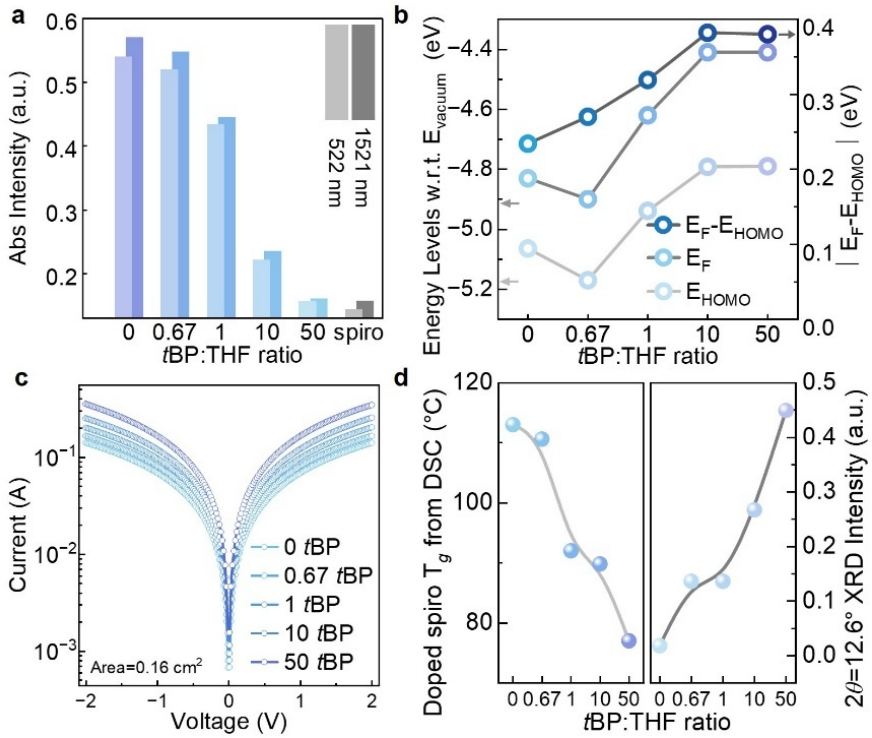

Fig. 3. Investigation of the role of *t*BP in the LODT process and optimization of HTL *via* its partial replacement with THF in different volume ratio. a, UV-Vis-NIR absorbance intensity changes of LODT-NH_4TFSI solutions prepared with different *t*BP to THF volume ratios, measured at wavelengths of 522 nm (light-colored bars) and 1521 nm (dark-colored bars). **b,** Fermi level (E_F) and the onset edge of the HOMO (E_{HOMO}) positions and their differences (| E_F – E_{HOMO} (eV) |, with respect to the vacuum level, E_{vacuum}) of the corresponding LODT-HTL films as a function of the *t*BP:THF volume ratios. **c,** Conductivity of LODT-HTL films with varying *t*BP concentrations (device structure of FTO/PEDOT:PSS/LODT-HTL/Au with an electrode area of 0.16 cm^2). **d,** Glass transition temperature (T_g) of the solid LODT-HTL and the relative intensity of the PbI_2 diffraction peak (2θ = 12.6°) under normalized intensity of the perovskite (110) peak from the XRD patterns as a function of *t*BP:THF ratio.

Furthermore, this de-doping phenomenon was corroborated by UV-Vis-NIR spectroscopy (**Fig. 3a**). We found that as the *t*BP concentration increased, the absorption intensities of the characteristic peaks for the oxidized spiro species (spiroTFSI) at 522 nm and 1521 nm decreased progressively, providing further evidence for the de-doping effect. An additional drawback of adding *t*BP is the reduction of the spiro-HTL's glass transition temperature, which compromises the thermal stability of the layer (**Fig. 3c**). However, despite these negative effects, we found that increasing *t*BP also enhanced the conductivity of the HTL film. Therefore, after carefully balancing these competing factors (electronic properties, doping efficiency,

thermal stability, and conductivity), we selected a 1:1 *t*BP/THF ratio as the optimal additive condition for the HTL in our final devices.

The relevant discussion is also added in our revised manuscript on Page 8, lines 174-194:

Incorporation of THF with *t*BP in LODT-HTL

The excellent doping ability of LODT also relies on the use of THF solvent. However, its rapid evaporation during spin-coating causes undesirable precipitation from NH_4TFSI, while adding *t*BP improves the film quality (**Fig. S11**). To gain the benefits and better understanding of *t*BP, it is necessary to investigate its specific role in LODT and the interaction with perovskite. Here, we take the resulting solid from LODT and then redissolved it in chlorobenzene (CB) to be consistent with conventional spiro solution. Meanwhile, to take advantage of THF, various amounts of THF are applied to replace *t*BP in the following studies.

As shown in **Fig. 3a** and **Fig. S12**, the absorption peaks of oxidized spiro at 522 nm and 1521 nm gradually decreased with increasing *t*BP/THF volume ratios. This indicates that *t*BP induces detrimental reactions with spiroTFSI, or promotes the de-doping of oxidized spiro. UPS characterization in **Fig. 3b** further corroborated the phenomena. LODT-HTL without *t*BP exhibited both deep Fermi level (E_F = ~-4.83 eV) and the highest occupied molecular orbital (E_{HOMO} = ~-5.06 eV) levels (with respect to the vacuum level, w.r.t. E_{vacuum}). Upon introducing a small amount of *t*BP (0.67:1 ratio), both E_F = ~-4.90 eV and E_{HOMO} = ~-5.17 eV dropped. With further increase in *t*BP, the E_F upshifted gradually, reaching a maximum of –4.41 eV at a 10:1 ratio, meanwhile the HOMO also shifted upward saturating at ~-4.79 eV. The widening of energy differences between the HOMO and E_F also suggests that *t*BP drives a de-doping effect in the pristine p-type LODT-HTL (**Fig. S13, S14**).[19]

(2) Thank you for the suggestion, which has indeed improved the clarity of the manuscript. We have now moved this part of the analysis into our revised version of our manuscript, incorporating **Fig. 3d** and move corresponding text to subsection: "**Integrating spiro-LODT HTL and TFSI additive in perovskite for photovoltaic devices**" The revised text from the previous version of the manuscript from Page 10, line 222 to Page 12, line 253 was moved to current version of the manuscript on Page 13, line 348 to Page 14, line 368.

1#2. From line 331-341, this paragraph illustrates the process of strengthening perovskite film by ATFSI (PEA or OA). I can see the discussion about OA and its GIXRD in Figure S22. But the discussion about PEA and Figure S23 and Figure S24 are in SI. Could the author move it to the main text? This would be helpful for readers to understand the story of the choice of large cation between OA and PEA.

Reply2:

Thank you for the suggestions. We have incorporated **Fig. 4h, i,** based on the data originally in **Fig. S22 and Fig. S23.** Additionally, we have incorporated the discussion originally in previous **Supplementary Note S2** in our revised version of the manuscript on Page 12, line 320 to Page 13, line 331:

Building on the established benefits of the $TFSI^-$ anion, we then explored the abilities of cations in TFSI additives: phenethylammonium (PEA^+) and OA^+ from PEATFSI and OATFSI, respectively. These cations form 2D-PVSK layers and behave different thermal stabilities. As shown in **Fig. 4h**, using grazing incidence X-ray diffraction (GIXRD, incident angle of ω = 1°), post-treatment with PEATFSI initially formed a 2D perovskite phase. However, this phase proved to be thermally unstable, decomposing upon heating, which is consistent with our previous finding[45] (**Fig. S43, S44**). This suggests ion exchange phenomenon between PEA^+ and FA^+ cations in TFSI additive and perovskite. In contrast, post-treatment with OATFSI yields a thermally robust 2D-PVSK layer. During heating, this 2D layer undergoes a stable phase evolution, transitioning from a n=2 phase (4.1°-4.2°) to a n=1 phase (3.2°) (**Fig. 4i, Fig. S45**). We attribute this superior stability to the larger size of the OATFI cation, which helps preserve the integrity of the 2D phase.

Supplementary Note S2 was removed in the revised version of the supporting information file.

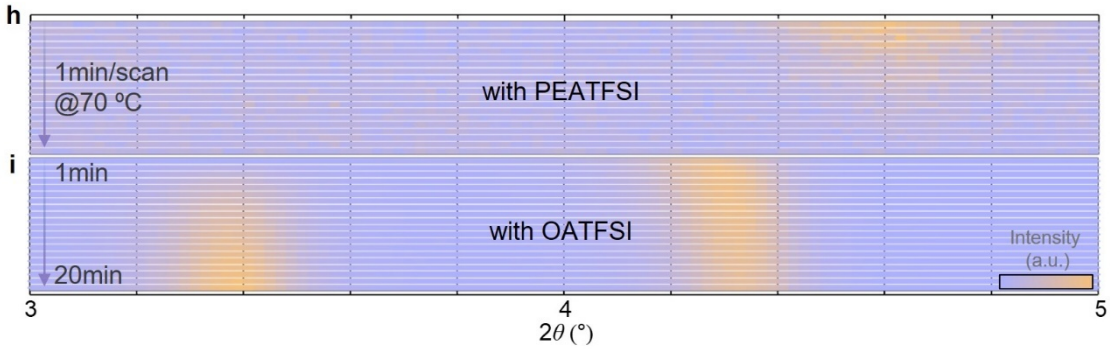

Fig. 4h, i, *In situ* grazing incidence X-ray diffraction (GIXRD, ω = 1°) monitoring the evolution of diffraction intensity as a function of angle every minute during annealing for $FAPbI_3$ perovskite films post-treated with **h,** PEATFSI and **i,** OATFSI for 20 min at 70 °C in air.

1#3. The manuscript focuses on the light-oxidation doping treatment (LODT) applied to spiro-OMeTAD in solution. Have the authors observed similar doping effects when LODT is applied directly to spiro-OMeTAD films? Furthermore, is it feasible to fabricate complete devices and then apply the LODT method post-fabrication to achieve comparable device performance? Clarification on this point would be valuable for understanding the practical applicability of the method.

Reply3:

Thank you for the enlightening comment. We have conducted new experiments to investigate this point. A spiro-HTL solution with NH_4TFSI was prepared in the dark to prevent pre-oxidation before being made into a film. We then applied light treatment directly to this solid-state film.

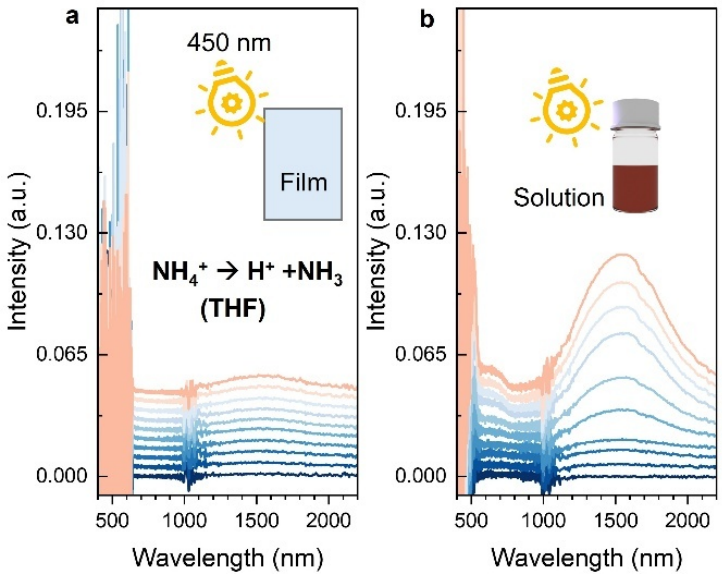

Voc	*Jsc*	FF	efficiency
9.12	2.33	48.1	10.2
9.27	2.40	60.7	13.5
9.20	2.47	49.8	11.3
8.38	2.57	50.7	10.9
8.21	2.47	53.7	10.9
9.08	2.32	48.9	10.3
9.19	2.38	61.1	13.4
9.12	2.43	51.8	11.5
8.81	2.41	32.5	6.9
9.00	2.55	44.2	10.1
8.90	2.47	36.1	8.1
8.30	2.62	46.0	10.0

Fig. R1. UV-Vis-NIR absorption spectra of the post treatment of LODT (450 nm as excitation wavelength) with NH_4TFSI on **a,** film and **b,** THF solution. Table shows the statistics of the post-treated HTL film on 5×5 cm^2 PSM with 8 sub-cell.

As shown in **Fig. R1a,** the UV-Vis-NIR absorbance of the film under illumination shows minimal change over time, whereas **Fig. R1b,** displays the rapid absorbance increase in the solution state for comparison. The accompanying table summarizes the performance statistics of the devices fabricated using this film post-treatment method. These results clearly demonstrate that, compared to the solution-based process, post-treating the solid-state film yields a much weaker response to light. This can be explained by the LODT mechanism. The doping of spiro by NH_4TFSI involves a reaction between spiro and free protons to form a spiro-HTFSI intermediate (Equation 1). Subsequently, a photo-excited spiro* molecule reacts with this intermediate to generate the oxidized spiroTFSI and hydrogen gas (Equation 2).

$$spiro + NH_4TFSI \rightarrow spiroHTFSI + NH_3 \qquad (1)$$

$$spiroHTFSI + spiro^* \xrightarrow{h\nu} spiro + spiro^{\cdot+}\,TFSI^- + {}^1/_2\,H_2 \qquad (2)$$

In the solid-state film, the dissociation and mobility of protons are severely restricted compared to in solution. This hinders the reaction, which is why no significant change in absorption intensity is observed.

Nevertheless, the corresponding devices exhibit some efficiency (**Fig. R1**, 10.6±1.87%), indicating that a certain degree of doping occurs during fabrication. We hypothesize this due to the high temperature during the gold electrode evaporation, which could thermally excite spiro* and further oxidize the spiro. Additionally, the low-vacuum environment might facilitate the outgassing of NH_3, resulting in the release of protons. However, overall, the doping efficiency of this post-treatment method is significantly low. These tests were a valuable investigation, and we are considering the development of suitable co-solvents for both spiro and ATFSI with lower volatility in our future work. This approach could prolong the solution-like state of spiro and ATFSI in the film state, which may allow post-fabrication treatments to play a more significant and effective role.

The above discussion has been incorporated in the revised version of our manuscript on Page 7, lines 153-161:

In LODT, the reaction can be presented as: $spiro + NH_4TFSI \rightarrow spiroHTFSI + NH_3$ and light accelerates the reaction of $spiroHTFSI + spiro^* \xrightarrow{hv} spiro + spiro^{\cdot+}\ TFSI^- + {}^1/_2\,H_2$. Here, the photoexcited spiro* readily transfers an electron to the proton, following with the reduction of proton to hydrogen, thereby generating the oxidized radical ($spiro^+$ or $spiro^{\bullet+}$) easily under suitable light activation (**Supplementary Note S1**). The resulting $spiro^+$ is stabilized by the $TFSI^-$ anion, while the deprotonated spiro species remains in the system and can further participate in subsequent reactions. Collectively, above results demonstrate that light irradiation is an effective method of accelerating the NH_4TFSI-induced oxidation of spiro in solution.

1#4. Can the authors provide time-resolved PL (TRPL), or space-charge limited current (SCLC) measurements of the perovskite films with and without KTFSI? These data would be very helpful for elucidating the impact of KTFSI on the optoelectronic properties and trap-state passivation of the perovskite layer.

Reply4:

Thank you for the valuable suggestion. We have supplemented the manuscript with both time-resolved photoluminescence (TRPL) and space-charge-limited current (SCLC) measurements to verify the passivation effect of KTFSI in perovskite. The results are now presented in **Fig. 4d,e**, **Fig. S32**, and **Fig. S33.**

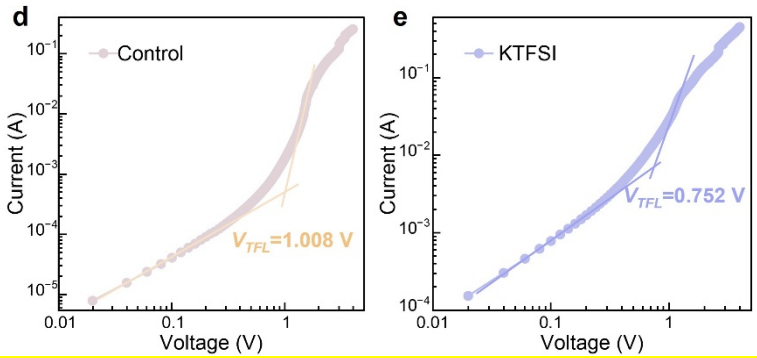

Fig. 4 d, e, Dark current–voltage (*I–V*) characteristics of the hole-only devices with FTO/PTAA/PVSK/spiro/Au configuration for **d**, control (PVSK with potassium iodide, KI) and **e**, PVSK with KTFSI (molar equivalent of KI). The trap-filled limit voltages (V_{TFL}) derived from the *I-V* curves are 1.008 V (control) and 0.752 V (KTFSI), respectively.

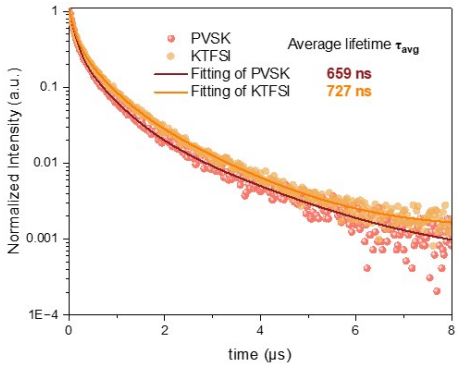

Fig. S32 Time-resolved photoluminescence (TRPL) decay of perovskite films. Comparison of TRPL decay curves and tri-exponential fits for perovskite films prepared with different potassium salts. The orange dots and fitting line represent the PVSK film treated with potassium iodide (KI), while the red dots and fitting line represent the PVSK film doped with KTFSI (molar equivalent of KI). The calculated average carrier lifetimes (τ_{avg}) are 659 ns and 727 ns for the control and KTFSI-doped films, respectively.

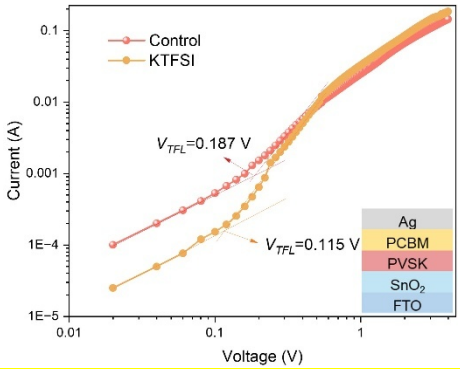

Fig. S33 Electron-only space-charge-limited current (SCLC) measurements. Dark current-voltage (*I-V*) characteristics of electron-only devices with FTO/SnO_2/PVSK/PCBM/Ag configuration employing

perovskite films with KI (Control, red dots) and KTFSI (orange dots). The trap-filled limit voltages (V_{TFL}) are determined to be 0.187 V and 0.115 V for the control and KTFSI-doped films, respectively.

Table S6. Fitting parameters for the time-resolved photoluminescence (TRPL) decay curves of different samples. The table lists the fast and slow component[S5],[S6] (time constants, τ_i, and relative amplitudes, A_i, from the TRPL decay curves) A tri-exponential function was used to fit the decays for perovskite films, while a bi-exponential function was used for the perovskite/HTL.

Sample	A_1	τ_1 (ns)	A_2	τ_2 (ns)	A_3	τ_3 (ns)	τ_{avg} (ns)
PVSK	0.724	113	0.279	423	0.048	1601	659
PVSK with KTFSI	0.582	107	0.344	437	0.106	1317	727
PVSK/Li-HTL	0.93	107	0.158	476	-	-	266
PVSK-KTFSI/Li-HTL	0.813	94	0.227	313	-	-	200
PVSK-KTFSI /mix OATFSI-HTL	0.807	93	0.236	299	-	-	193

The above discussion have been incorporated in the revised version of our manuscript on Page 11, lines 269-276.

Time-resolved photoluminescence (TRPL) measurements in **Fig. S32 (Table S6)**, show a slower charge carrier decay in the KTFSI-doped perovskite, further indicating less defects compared to the pristine perovskite film. The benefit of KTFSI doping was also quantified by space-charge-limited current (SCLC) measurements (**Fig. 4d,e and Fig. S33**), which demonstrated a reduction of trap state density for both electrons (from 2.83×10^{14} cm^{-3} to 1.74×10^{14} cm^{-3}) and holes (from 1.52×10^{15} cm^{-3} to 1.14×10^{15} cm^{-3}), confirming the superior quality of the KTFSI-modified perovskite films.

1#5. It would further enrich the manuscript if the authors could compare the charge transfer dynamics between the traditional doping strategy and the LODT approach. For instance, TRPL or transient absorption (TA) spectroscopy on perovskite/HTL stacks could provide insight into the interfacial carrier dynamics and efficiency of hole extraction in both scenarios.

Reply5:

Thank you for the suggestion. We have supplemented the manuscript with both TRPL and TAS measurements to verify the doping effect in LODT-HTL. The results are now presented in **Fig. S40, Fig. 2e,f, Fig. S10** and **Fig. S56.**

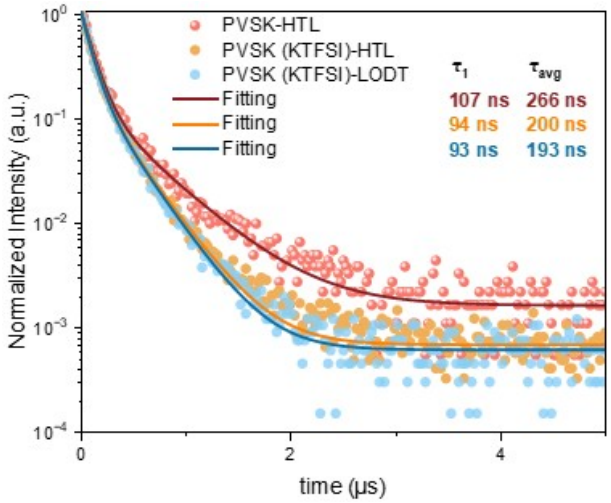

Fig. S40 TRPL curves with bi-exponential fits of conventional LiTFSI doped spiro (HTL) on pristine perovskite (PVSK-HTL, red dots), HTL on KTFSI modified perovskite [PVSK(KTFSI)-HTL, orange dots], and LODT-OA (co-doped NH_4TFSI with 1% mol OATFSI) on KTFSI modified perovskite [PVSK(KTFSI)-LODT, blue dots] deposited on quartz substrates, comparing different interfacial carrier dynamics.

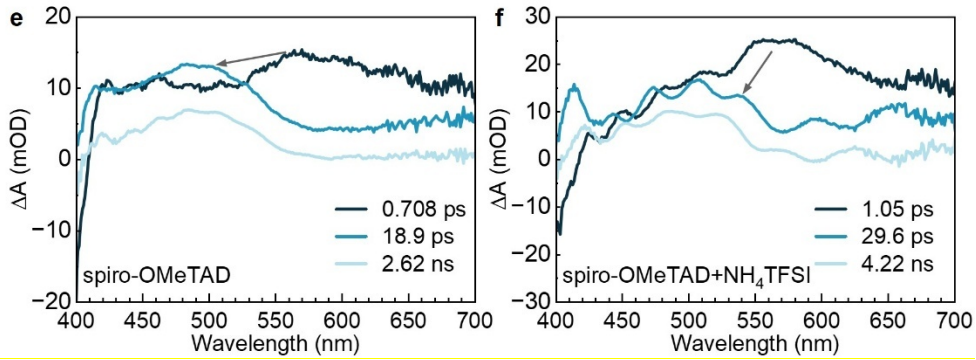

Fig. 2e, f, Decay-associated spectra (DAS) for a pristine spiro film and NH_4TFSI doped spiro film. The DAS were obtained from transient absorption spectra (TAS) by global fitting with a tri-exponential function.

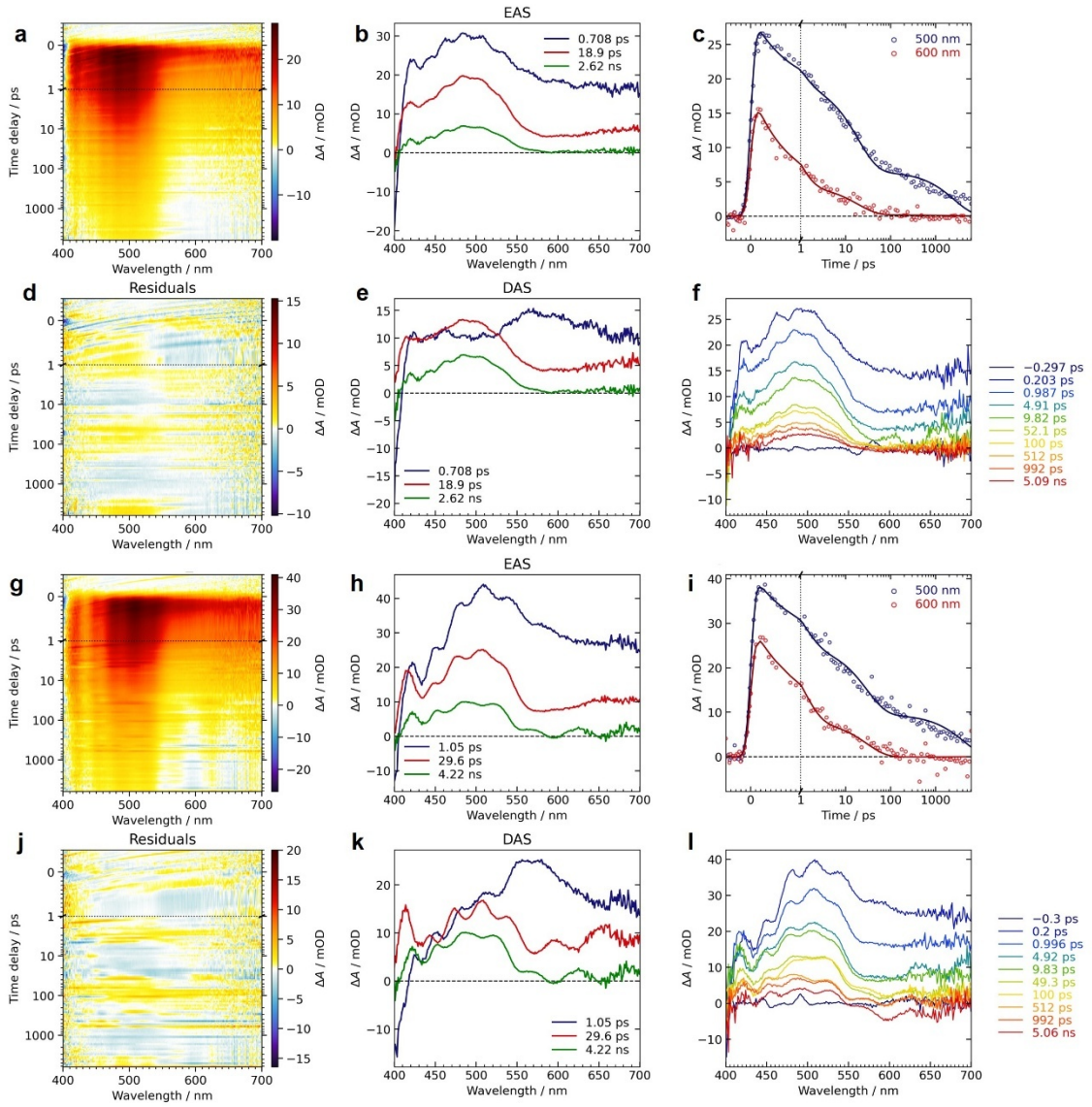

Fig. S10. Pump-probe transient absorption spectroscopy (TAS) of pristine and NH_4TFSI-doped spiro-HTL. Comprehensive TA data and global analysis for a pristine spiro-OMeTAD film (**a-f,**) and an NH_4TFSI-doped LODT-HTL film (**g-l,**), following excitation with a 350 nm pump pulse. **a, g,** Chirp-corrected transient absorption data displayed as contour plots. **b, h,** Evolution-associated spectra (EAS). **c, i,** Experimental (circles) and fitted (solid lines) kinetic traces at representative wavelengths. **d, j,** Residuals matrix from the global fit. **e, k,** Decay-associated spectra (DAS). **f, l,** Transient absorption spectra at selected time delays.

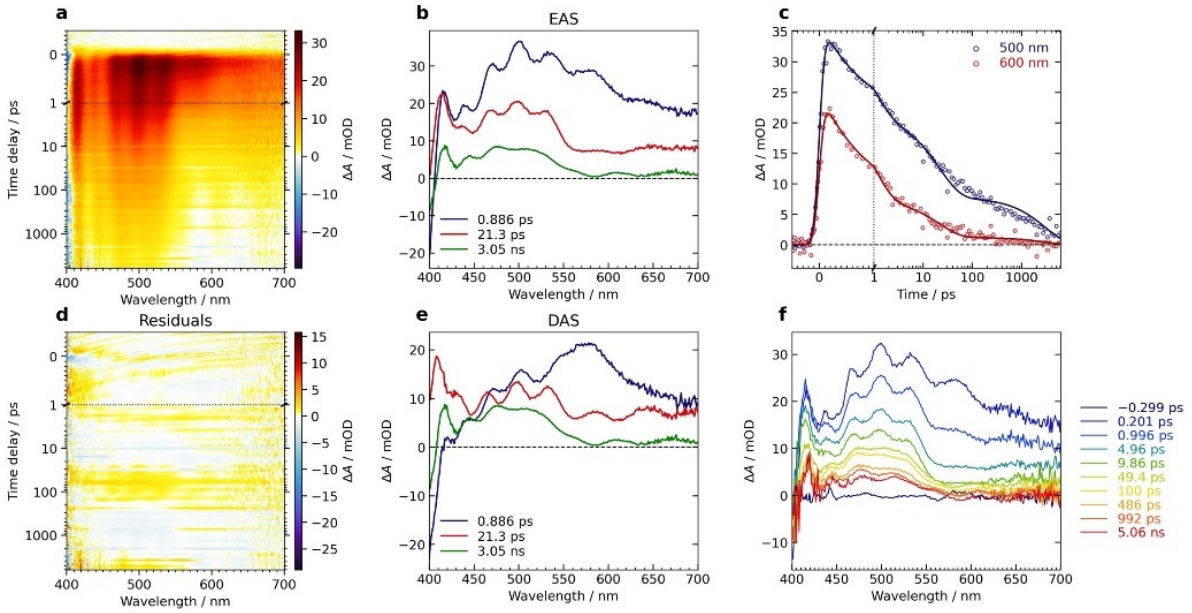

Fig. S56. **Pump-probe transient absorption spectroscopy (TAS) of co-doped OATFSI in LODT-HTL with NH_4TFSI under excitation with a 350 nm pump pulse.** Comprehensive TA data and global analysis for a pristine spiro-OMeTAD film. **a,** Chirp-corrected transient absorption data displayed as contour plots. **b,** Evolution-associated spectra (EAS). **c,** Experimental (circles) and fitted (solid lines) kinetic traces at representative wavelengths. **d,** Residuals matrix from the global fit. **e,** Decay-associated spectra (DAS). **f,** Transient absorption spectra at selected time delays.

We have incorporated the above new results in the revised version of our manuscript and supplementary information files. In addition, the following revisions have been made in the revised manuscript:

On Page 12, lines 311-314, the TRPL results are described.

To further investigate the interfacial role of TFSI, we analyzed the perovskite/HTL interface by TRPL. The incorporation of KTFSI was found to accelerate charge carrier extractions, where the fast decay component (τ_1) decreased from 107 ns to 94 ns (**Fig. S40, Table S6**).

On Page 7, line 161 to Page 8, line 172, the TAS results are described.

Then, we performed femtosecond transient absorption spectroscopy (TAS) to study the oxidation activation process under the light exposure. Pristine spiro-HTL exhibited a broad peak in the range of 420-550 nm (**Fig. S10f**). After doping with NH_4TFSI, an additional response emerged within 560-610 nm (**Fig. S10l**), characteristic of the excited state spiro* species.[36],[39] This indicates that pristine spiro, without $TFSI^-$, cannot efficiently undergo the excitation-induced oxidation (spiro* → $spiro^+$). Decay-associated spectra (DAS) further support that and the analysis with triple-exponential fitting revealed that LODT-HTL

undergoes a distinct decay pathway leading to oxidized radical cations, indicated by a prominent 530 nm feature from spiroTFSI. In contrast, no similar signature was observed for the pristine spiro (**Fig. 2e, f**), suggesting the effective doping of spiro-HTL.

Additional discussion was added on Page 14, lines 371-373.

DAS analysis showed that the addition of OATFSI enhanced photo-excitation process of HTL, reducing the time from 29.6 ps to 21.3 ps corresponding to the NH_4TFSI only HTL (**Fig. S56, Fig. S10**).

1#6. When discussing dopants for spiro-OMeTAD, the authors are encouraged to engage more thoroughly with recent literature to acknowledge key developments in the field. In particular, we recommend that the authors review and cite the following significant contributions, which offer a comprehensive overview of progress and insights into molecular doping strategies:

https://doi.org/10.1016/j.mser.2024.100875 (2025)

https://pubs.rsc.org/en/content/articlehtml/2021/ee/d1ee02095a (2021)

https://pubs.rsc.org/en/content/articlelanding/2021/ta/d0ta11564a (2020)

https://pubs.rsc.org/en/content/articlehtml/2019/sc/c8sc05284k (2019)

Reply6:

Thank you for the suggestion. After carefully reading and integrating these references, we affirm that these four articles have broadened our understanding of the field and deepened our knowledge of spiro-OMeTAD modification, additives, and doping strategies. Consequently, we have added the above new citations into our revised manuscript:

References:

[28] (https://doi.org/10.1016/j.mser.2024.100875) on Page 5, line 88.

[35] (https://pubs.rsc.org/en/content/articlehtml/2021/ee/d1ee02095a) on Page 5, line 88.

[17] (https://pubs.rsc.org/en/content/articlelanding/2021/ta/d0ta11564a) on Page 4, line 70.

[18] (https://pubs.rsc.org/en/content/articlehtml/2019/sc/c8sc05284k) on Page 4, line 70.

Thank you again for the recognition of our work. In responding to the comments and supplementing the new experimental results have given us a more thorough understanding of the role of *t*BP in the LODT-HTL. The additional TRPL and TAS experiments have also allowed us to more clearly elucidate the effect and mechanism of the dopants. Furthermore, adopting the reviewers' suggestions to restructure the manuscript has enabled us to better express our core ideas and the focus of our work: namely, to elucidate the advantages of versatile TFSI additives, investigate their role in the LODT-HTL, and decouple the effects of their anions and cations on the perovskite surface.

Response to Reviewer #2

In this work, Zhang et al. developed a light-induced doping strategy for Spiro-OMeTAD that eliminated the need for post-oxidation by triggering the spontaneous generation of protons in the Spiro-OMeTAD solution. This approach also enabled the construction of Li-free Spiro-OMeTAD-based perovskite solar cells by replacing LiTFSI with a series of synthesized ammonium TFSI salts. Additionally, they introduced TFSI salts into perovskite films, which promoted the growth of larger grains with fewer surface defects. Through synergistic regulation of both the HTL and perovskite layers using TFSI salts, they achieved highly efficient and stable perovskite solar cells. While the use of ammonium TFSI salts to dope Spiro-OMeTAD is novel, the light-induced doping method has been widely reported (e.g., Joule 2024, 8, 1707; Nature 2021, 594, 51). Thus, the authors should clearly highlight the advantages of their proposed strategy compared to these pioneering studies. Further technical comments are provided below.

In light of these concerns, I recommend that the authors address the critical issues and make the necessary revisions before the manuscript can be considered for further evaluation.

Reply:

Thank you for the valuable comments and suggestions, which help further improve our manuscript. We have carefully read them. Below please find our point-by-point responses. For your convenience, the major changes we have made in the manuscript and the SI are highlighted in yellow.

After a careful literature review and comparison with prior works, we wish to highlight our perspective and clarify the novelty of our approach. Regarding the pioneering work in previous reference **[25]** on Page 4, line 84 that uses CO_2 in a light-induced doping method, we emphasize that while it effectively uses CO_2 as an oxidant for photo-excited spiro*, the system still relies on the hygroscopic LiTFSI salt. Furthermore, the requirement of an external CO_2 gas supply, although seemingly more efficient than oxygen, may pose limitations for large-scale applications. We have clarified this distinction in our revised manuscript (Page 4, lines 75-77 as: Another strategy involves photo-activated oxidation through CO_2 reduction,[25] providing an additional doping pathway, but it remains dependent on the hygroscopic LiTFSI.[26]

Another highly relevant study (Joule 2024, 8, 1707) reported a light-induced, symmetry-breaking oxidation, while not requiring external gas, was dependent on the participation of *t*BP. That work shared the same initial motivation as ours: the observation of color change and doping in a conventional LiTFSI-spiro solution after light exposure. Later on, they mainly focus on the mechanism of Y^{3+}-*t*BP or La^{3+}-*t*BP reacting with spiro under light by so-called symmetry-breaking oxidation pathway. However, the authors of that study also explicitly noted that the mechanism of LiTFSI was different from their proposed symmetry-

breaking oxidation, suggesting a more complex underlying mechanism. In our original manuscript, our proposed mechanism based on ^{1}H NMR results was potentially inappropriate as it overlooked the critical role of *t*BP. We have revised our discussion from previous Page 7, lines 122-179, and emphasizing the recent findings on Page 6, lines 109-113 of our revised manuscript: Distinguished from the LiTFSI and *t*BP involving photooxidation process,[36],[37] protons can effectively react with spiro (**Supplementary Note S1**). Most inorganic ammonium compounds can gradually release protons in solution, depending on their acid dissociation constant (pK_a). Thus, the proton-containing ammonium cations in TFSI additives were studied.

Additional highlights are summarized below emphasizing further the novelty and importance of our work:

(1) A simplified doping system: The primary novelty is the use of ammonium TFSI (ATFSI) salts as dopants that react with photo-activated spiro* under anhydrous and anaerobic conditions. This reaction requires neither external gases (like CO_2 or O_2) nor the chemical participation of *t*BP. We have shown that the role of *t*BP is solely to improve the film quality of the spiro-HTL by acting as a processing additive.

(2) Application of simpler additives: We have compiled previous studies that have used ATFSI salts as additives (**Table S14**). Notably, these prior works do not mention or imply a photo-doping mechanism. The innovation of our work lies in the discovery that photo-doping is a highly effective and previously unrecognized activation mechanism for these simpler ATFSI salt systems.

Table S14. Summary of recent studies on the use of ATFSI salts as dopants for spiro-OMeTAD hole transport layers. The use of TMATFSI as a dopant has not been previously reported to the best of our knowledge. LODT: Light oxidation doping treatment.

ATFSI additive	LODT	Composition of HTL	Reference
MATFSI	No	6 mg MATFSI/36 µL *t*BP 91.4 mg spiro-OMeTAD	[S11]
DMATFSI	No	2% DMATFSI/9.1 mg LiTFSI/28.8 µL *t*BP 75 mg spiro-OMeTAD	[S12]
TMATFSI	-	-	-
TeMATFSI	No	6.42 mg TeMATFSI/17 µL *t*BP 43.4 mg spiro-OMeTAD	[S13]
OATFSI	No	24 mM OACl/24 mM LiTFSI 70 mM spiro-OMeTAD	[S14]

(3) Design strategy for cations and anions in ATFSI salts: Beyond the HTL, our work introduces a holistic strategy by decoupling the distinct roles of cations and anions in the ATFSI salts to synergistically modulate both the HTL and the perovskite surface leading to improvements in device efficiency and stability.

2#1. It seems that the authors employ tBP as an additive for doping Spiro-OMeTAD via the LODT strategy. However, several critical details require clarification:

(1)Was tBP added during the LODT Spiro-HT solution preparation, or only afterward?

(2)If tBP was omitted, could CB/THF alone dissolve the synthesized ammoniumTFSI?

(3)Is tBP merely a processing aid (solubilizer) or does it actively participate in doping?

Reply1:

Thank you for raising the above three important points.

(1) The *t*BP is only added after the LODT preparation steps. We apologize for not clearly pointing out the *t*BP function and the preparation method of *t*BP when added in spiro-HTL. We have added a separate paragraph describing the spiro-HTL preparation sequence in the revised version of our supplementary information file on Page 3, line 78 to Page 4, line 91:

Preparation of LODT-HTL:

72 mg spiro-OMeTAD and synthesized ammonium TFSI salt (or LiTFSI) were dissolved in 1 mL of mixed solvents with CB : THF=100:1 (V:V). Then, the solution was irradiated by UV light (350 nm) for around 5 min until there is no longer a noticeable change of its color. Excessive volume of hexane was added in order to precipitate the oxidized spiro. After filtering, dark brown colored oxidized spiro solids were obtained, which were washed with EA and hexane to remove water and then dried overnight in vacuum oven at 50 °C. All processes were carried out in N_2 glove box. Alternatively, the reaction product can be collected as a solid powder to facilitate handling and storage for a long period. To do this, we changed the solvent from chlorobenzene to chloroform. Despite the changes in solvents, the solution preparation procedure was the same unless otherwise noted. The weighted amount of 0.059 mol of solid was mixed with CB and THF with 100:1 (V:V), then *t*BP with a volume of 1:1 (V:V) *t*BP:THF was added, without subsequent filtration.

(2) Yes, CB/THF alone can dissolve the synthesized ammonium TFSI (**Fig. R2a,b**). The related description can be found in the revised version of supplementary information file, section "**Preparation of LODT HTL**" and **Fig. S1.** THF was found to dissolve both NH_4TFSI and LiTFSI effectively.

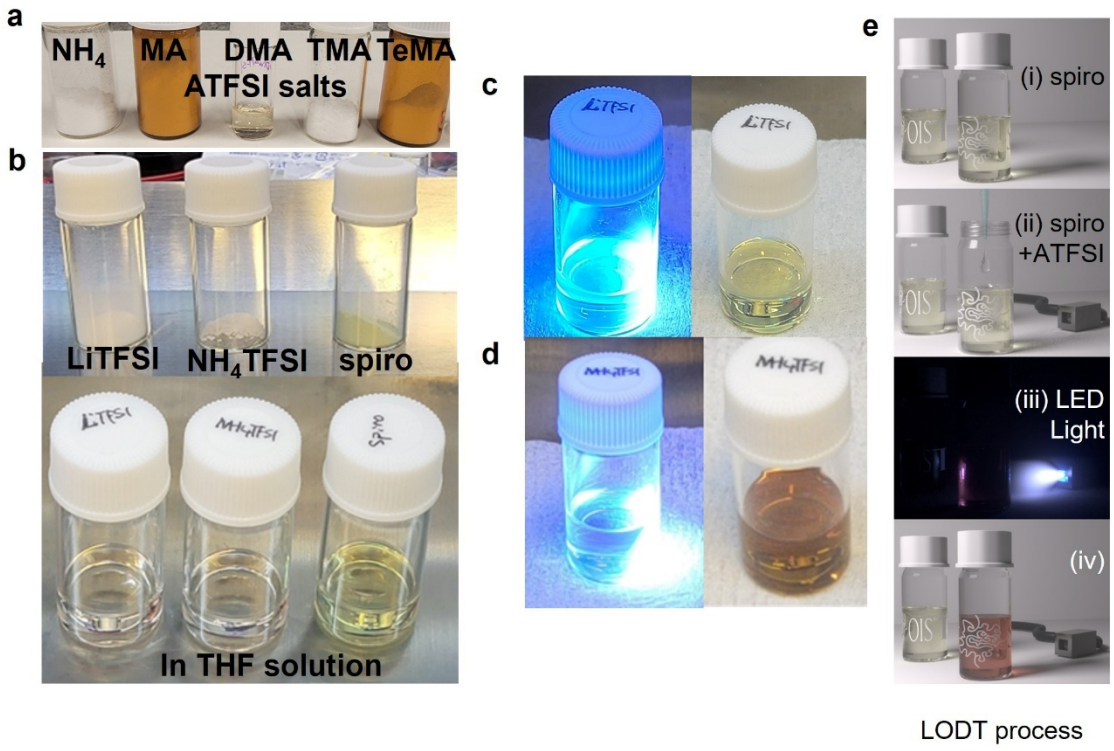

Fig. R2. Photos of the synthesized ATFSI salts and corresponding solutions in THF. a As-synthesized ATFSI salts. NH_4TFSI, MATFSI, and TMATFSI are white solids, whereas DMATFSI appears as an ionic liquid. **b** Solutions after dissolving LiTFSI, NH_4TFSI and spiro-OMeTAD in THF. **c,** The LODT of LiTFSI with spiro in CB/THF and **d,** The LODT of NH_4TFSI with spiro in CB/THF in N_2 glovebox (H_2O and O_2 < 0.1 ppm). **e,** Schematic illustration of the experimental procedure for the LODT method. Steps (i)-(iv) visually demonstrate the oxidation of spiro in solution through the varying color change observed after adding different ATFSI to a spiro/THF solution followed by light exposure.

The above new contents were incorporated as **Fig. S1** and **Fig. 2a**.

(3) The *t*BP additive is merely a solubilizer. However, our studies show the de-doping effect in LODT-HTL with increasing amounts of *t*BP. The related description can be found on Page 8, line 174 to Page 9, line 200:

Incorporation of THF with *t*BP in LODT-HTL

The excellent doping ability of LODT also relies on the use of THF solvent. However, its rapid evaporation during spin-coating causes undesirable precipitation from NH_4TFSI, while adding *t*BP improves the film quality (**Fig. S11**). To gain the benefits and better understanding of *t*BP, it is necessary to investigate its specific role in LODT and the interaction with perovskite. Here, we take the resulting solid from LODT and then redissolved it in chlorobenzene (CB) to be consistent with conventional spiro solution. Meanwhile,

to take advantage of THF, various amounts of THF are applied to replace *t*BP in the following studies. As shown in **Fig. 3a** and **Fig. S12**, the absorption peaks of oxidized spiro at 522 nm and 1521 nm gradually decreased with increasing *t*BP/THF volume ratios. This indicates that *t*BP induces detrimental reactions with spiroTFSI, or promotes the de-doping of oxidized spiro. UPS characterization in **Fig. 3b** further corroborated the phenomena. LODT-HTL without *t*BP exhibited both deep Fermi level (E_F = ~-4.83 eV) and the highest occupied molecular orbital (E_{HOMO} = ~-5.06 eV) levels (with respect to the vacuum level, w.r.t. E_{vacuum}). Upon introducing a small amount of *t*BP (0.67:1 ratio), both E_F = ~-4.90 eV and E_{HOMO} = ~-5.17 eV dropped. With further increase in *t*BP, the E_F upshifted gradually, reaching a maximum of –4.41 eV at a 10:1 ratio, meanwhile the HOMO also shifted upward saturating at ~-4.79 eV. The widening of energy differences between the HOMO and E_F also suggests that *t*BP drives a de-doping effect in the pristine p-type LODT-HTL (**Fig. S13, S14**).[19] Considering the interaction between *t*BP and NH_4TFSI-spiro, we can explain why first a downshift of both WF and E_{HOMO} at ratio of 0.67 *t*BP is observed. This is because even a trace amount of *t*BP can induce the formation of spiro aggregates, creating donor-acceptor complexes that cause the WF and E_{HOMO} to shift to deeper energy levels.[40] However, as more *t*BP is added, its more dominant de-doping effect takes over, causing the apparent WF and E_{HOMO} to shift back to shallower energy levels and increasing the energy differences of $|E_F\text{-}E_{HOMO}|$ as shown in **Table S2**.

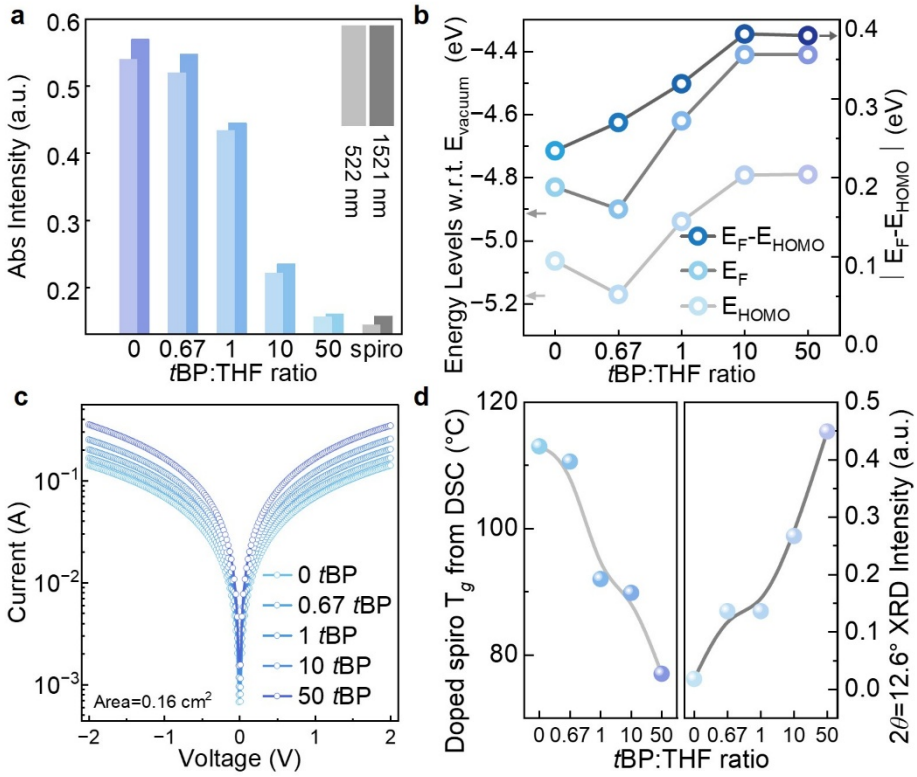

Fig. 3. Investigation of the role of *t*BP in the LODT process and optimization of HTL *via* its partial replacement with THF in different volume ratio. a, UV-Vis-NIR absorbance intensity changes of LODT-NH_4TFSI solutions prepared with different *t*BP to THF volume ratios, measured at wavelengths of 522 nm (light-colored bars) and 1521 nm (dark-colored bars). **b,** Fermi level (E_F) and the onset edge of the HOMO (E_{HOMO}) positions and their differences ($| E_F - E_{HOMO}$ (eV) $|$, with respect to the vacuum level, E_{vacuum}) of the corresponding LODT-HTL films as a function of the *t*BP:THF volume ratios. **c,** Conductivity of LODT-HTL films with varying *t*BP concentrations (device structure of FTO/PEDOT:PSS/LODT-HTL/Au with an electrode area of 0.16 cm^2). **d,** Glass transition temperature (T_g) of the solid LODT-HTL and the relative intensity of the PbI_2 diffraction peak (2θ = 12.6°) under normalized intensity of the perovskite (110) peak from the XRD patterns as a function of *t*BP:THF ratio.

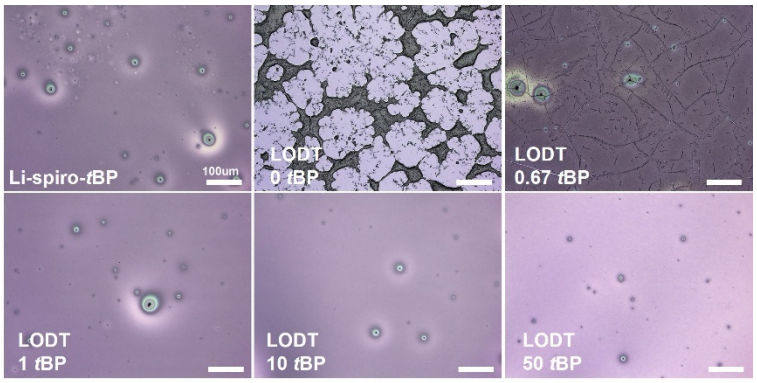

Fig. S11. Effect of *t*BP/THF volume ratio on the film morphology of LODT-HTLs. Optical microscopy images of conventional LiTFSI-doped spiro-HTL and NH_4TFSI-doped LODT-HTL films prepared with varying volume ratios of *t*BP:THF. All scale bars correspond to 100 μm.

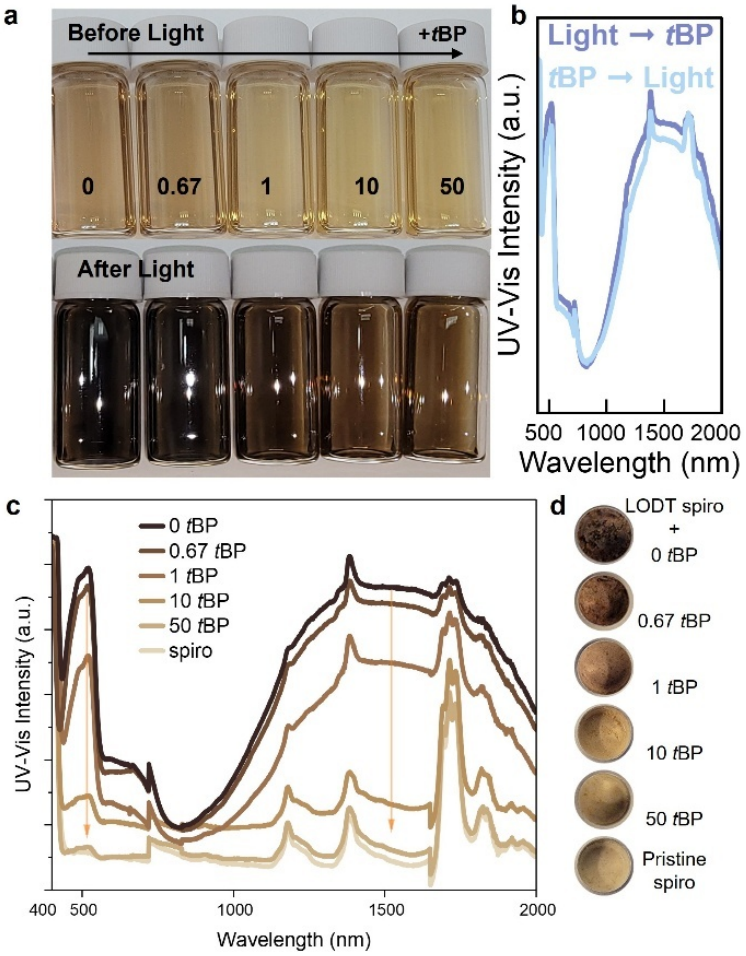

Fig. S12. Effect of *t*BP addition on the optical properties of LODT solutions. a, Photos of spiro solutions prepared with varying amounts of *t*BP added before and after being illuminated with white light. **b,** Comparison of the final solution absorbance resulting from two different process sequences: adding *t*BP before light exposure and adding it after. **c,** Corresponding UV-Vis-NIR absorption spectra for the solutions shown in **a. d,** Photos of the solid materials that remained after solvent evaporation. NH_4TFSI was employed as dopants for all LODT-HTL solutions.

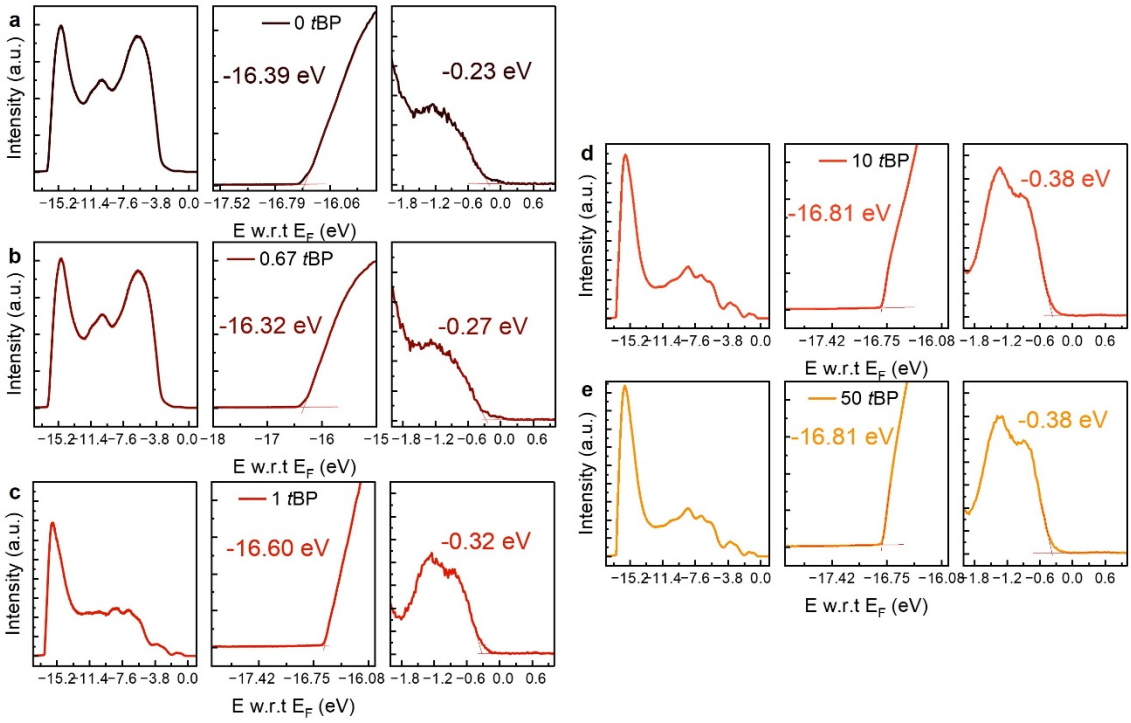

Fig. S13 Effect of the *t*BP concentration on the energy levels of LODT-HTL films, studied by UPS. UPS spectra of NH_4TFSI-doped LODT-HTL films prepared with varying volume ratios of *t*BP to THF. The *t*BP/THF ratios for the respective panels are: **a,** 0, **b,** 0.67, **c,** 1, **d,** 10, and **e,** 50. For more information see **Table S2.**

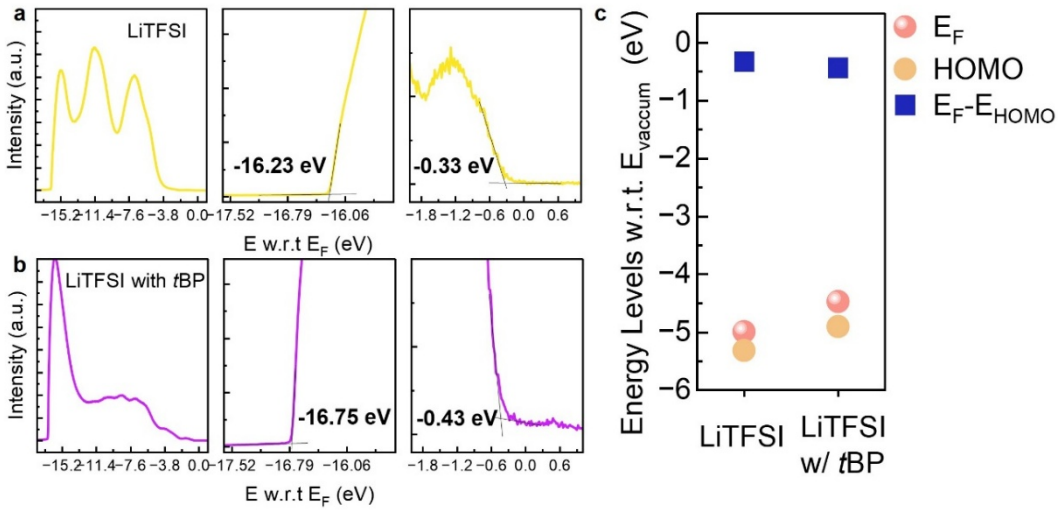

Fig. S14 Effect of the *t*BP on the energy levels of conventionally LiTFSI-doped spiro-HTL films. a, b, UPS spectra of LiTFSI-doped spiro-HTL films prepared **a,** without and **b,** with the addition of *t*BP in THF solvent. **c,** Summary and comparison of the corresponding E_F, HOMO position, and their energy differences ($|E_F - E_{HOMO}|$).

Table S2. Summary of the Fermi level (E_F), HOMO (E_{HOMO}) level, and energy difference (| E_F–E_{HOMO} |) (w.r.t. E_{vacuum} = 0 eV) for spiro-HTL films doped with various *t*BP ratios in NH_4TFSI doped LODT-HTL.

Condition	E_F (eV) (w.r.t. E_{vacuum})	E_{HOMO} (eV) (w.r.t. E_{vacuum})	| E_F-E_{HOMO} | (eV)
0 *t*BP	-4.83	-5.06	0.23
0.67 *t*BP	-4.90	-5.17	0.27
1 *t*BP	-4.62	-4.94	0.32
10 *t*BP	-4.41	-4.79	0.38
50 *t*BP	-4.41	-4.79	0.38

Table S3. Conductivity of NH_4TFSI-doped LODT-HTL films with different *t*BP concentration. The measurements were conducted on devices with the structure FTO/PEDOT:PSS/spiro-OMeTAD/Au. The thickness of the spiro-OMeTAD film was 240 nm and the electrode area was 0.09 cm^2.

Film	Conductivity ($\times 10^{-3}$ S/cm)
spiro	2.384×10^{-4}
0 *t*BP	1.879
0.67 *t*BP	2.270
1 *t*BP	2.674
10 *t*BP	3.447
50 *t*BP	4.679

Table S4. Sheet resistance (R_{sq}) of NH_4TFSI-doped LODT-HTL films with different *t*BP concentration. The measurements were performed using the four-point probe method on samples with an ITO/spiro-OMeTAD structure. The thicknesses of the spiro-OMeTAD and ITO layers were 240 nm and 60 nm, respectively.

Film	R_{sq} (Ω/□)
ITO	11.947 ± 0.028970
0.67 *t*BP	10963 ± 22.021
1 *t*BP	10936 ± 22.630
10 *t*BP	10881 ± 4.8099
50 *t*BP	10822 ± 19.599

2#2. If the authors used tBP as an additive for doping Spiro-OMeTAD through their LODT strategy. To properly evaluate this work's contribution, the manuscript should clearly compare this approach with established doping methods from previous studies (DOI: 10.1126/science.abo2757; DOI: 10.1038/s41467-024-52199-4; DOI: 10.1002/anie.202316183).

Reply2:

Thank you for the comment. We apologize for not being clear about statement of *t*BP usage in LODT preparation, the *t*BP were not involved in the LODT doping step, but were only added afterwards.

We have made further clarifications on this point on Page 8, lines 175-182:

The excellent doping ability of LODT also relies on the use of THF solvent. However, its rapid evaporation during spin-coating causes undesirable precipitation from NH_4TFSI, while adding *t*BP improves the film quality (**Fig. S11**). To gain the benefits and better understanding of *t*BP, it is necessary to investigate its specific role in LODT and the interaction with perovskite. Here, we take the resulting solid from LODT and then redissolved it in chlorobenzene (CB) to be consistent with conventional spiro solution. Meanwhile, to take advantage of THF, various amounts of THF are applied to replace *t*BP in the following studies.

2#3. The authors claimed "the higher XRD intensity indicated improved crystallinity" in Line 282, which seems to be not inaccurate. XRD intensity depends on multiple factors including instrumental parameters.

Reply3:

We agree with your point that the peak intensity alone cannot be directly used to assess crystallinity. Therefore, in the revised manuscript we have added a detailed discussion on the full width at half maximum (FWHM) of the XRD peaks. Since narrower diffraction peaks (smaller FWHM) correspond to larger grain sizes and better long-range order, the FWHM is a more reliable indicator of crystallinity than peak intensity. We repeated the experiments depositing the perovskite films based on the two-step deposition method. As shown in the revised **Fig. S20**, the (110) peak of the KTFSI-modified perovskite films exhibits a significantly reduced FWHM compared to the pristine perovskite (**Table S5**), confirming the improved grain growth and higher crystallinity. This provides evidence to support our conclusion regarding enhanced crystal quality. Moreover, since the same XRD instrument (**Supplementary Information** Page 7, lines 184-186: **Characterization methods**: X-ray diffraction measurements were carried out on a Bruker D8 Discover diffractometer (Bruker AXS) using a Cu (λ = 1.54 Å) source with a power output of 1600 W.) and measurement parameters were applied for all samples, we believe that comparing the FWHM values provides a more accurate evaluation of the crystallinity of the perovskite films.

The revised contents are on Page 10, lines 238-243:

In particular, the beneficial influences of KTFSI were evident in the two-step method, where the grain size grew from less than 500 nm to over 1 μm. Additionally, the corresponding XRD showed a notable higher intensity at (110) and (220) peak position (**Fig. S20 and Table S5**). The reduced full width at half maximum (FWHM) indicates improved crystallinity after the formation of perovskite phase with KTFSI doping.

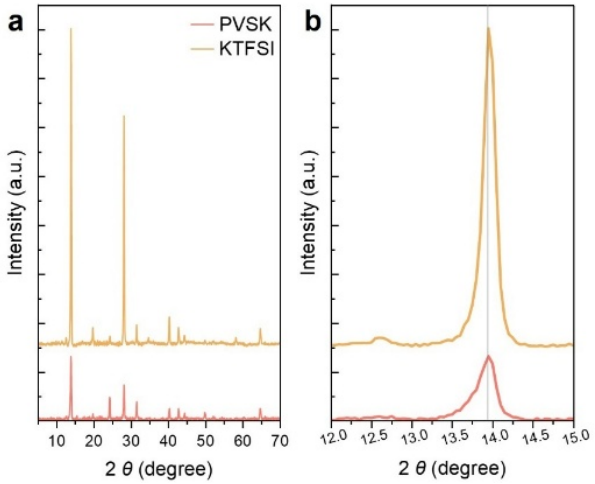

Fig. S20. XRD analysis of the effect of KTFSI on two-step processed perovskite films. Comparison of XRD patterns for pristine (control) and KTFSI-doped perovskite films. **a,** Wide-angle scan over the 2-theta range of 2θ = 5-70°. **b,** Zoomed-in view of the 2θ = 12-15° region, highlighting the main PbI_2 (100) peak ($2\theta \sim 12.6°$) and the perovskite (110) peak ($2\theta \sim 14.1°$).

Table S5. Comparison of XRD peak parameters for pristine and KTFSI-doped perovskite films corresponding to PbI_2 (100) and $FAPbI_3$ (110). The table summarizes the peak intensity, peak area, and FWHM values for the diffraction peaks corresponding to the PbI_2 and the main perovskite phases.

Sample	2-Theta (degree)	Area	FWHM (degree)
Pristine perovskite	12.643	34.5	0.354
	13.945	802.6	0.31
With KTFSI	12.611	71.2	0.214
	13.957	2858.9	0.187

2#4. The retarding effect of TFSI on the FAI-PbI2 reaction kinetics, and its consequent impact on grain growth, requires further mechanistic clarification. Could the authors discuss potential chemical interactions or phase evolution data supporting this observation?

Reply4:

Thank you for the comment. As the reviewer suggested, we have added new clarifications on the evolution of perovskite layer crystallization modulated by KTFSI. We employed time-resolved SEM (**Fig. R3a**) and excitation-emission matrix (EEM) fluorescence spectroscopy (**Fig. R3b**) to monitor the evolution of the perovskite film properties at different annealing times. We found that KTFSI regulates the growth of the perovskite film (**Fig. R3a**). This is supported by the EEM results (**Fig. S31**), which show a delayed onset but ultimately with a much stronger emissive intensity, indicating a more controlled crystallization process with lower trap density corroborated by the SCLC measurements (**Fig. 33**). Furthermore, we observed that adding KTFSI significantly affects the perovskite both in precursor solution and crystallization behaviors as shown in **Fig. S27-S29**. Specifically, the comparison of optical microscopy images reveals a significant difference in the morphology of crystals grown from the DMF/DMSO solution after the addition of KTFSI. Due to the hydrophobic nature of the -CF_3 groups in the $TFSI^-$ anion, the precursor solution containing KTFSI first aggregates into uniformly dispersed droplets. Crystallization then proceeds within these droplets, a process which effectively prevents the formation of uncontrolled dendrites. This observation also suggests an interaction between the $TFSI^-$ anion and the perovskite intermediate phase during film formation. Based on these new findings, we have proposed a mechanism for KTFSI-mediated perovskite film growth (**Fig. R3c**) in the revised version of our manuscript on Page 10, line 243 to Page 11, line 269:

To elucidate the role of KTFSI in the perovskite film formation, we tracked the morphological evolution during annealing. SEM images (**Fig. 4a, Fig. S21-24**) revealed that KTFSI significantly promotes grain growth *via* an Ostwald ripening process, resulting in larger, smoother grains compared to the pristine film yet without affecting the final optical properties (**Fig. S25**). KTFSI was found to enhance the crystallinity of the PbI_2 film in the two-step deposition, evidenced by XRD of FWHM at the (001) peak for PbI_2 from 0.119 to 0.079 (**Fig. S26**), while also creating a significant porous structure. Such morphology facilitates the complete conversion from PbI_2 to perovskite upon reaction with FAI, as confirmed by the near elimination of the residual PbI_2 peak (**Fig. S22b**). We also attribute this enhanced crystallinity to a mechanism where $TFSI^-$ anions interact with FAI and PbI_2, retarding the typically rapid PbI_2-FAI reaction. This controlled reaction is related with several factors: potential hydrogen bonds may form between the -CF_3 groups on the $TFSI^-$ and the formamidinium cation (FA^+),[43] meanwhile the oxygen on the $TFSI^-$ can coordinate with Pb^{2+}. These interactions create a form of steric hindrance, making the direct and rapid reaction between FAI and PbI_2 more difficult and slower.[44] As the film is heated, the FAI gains enough energy to overcome the binding energy of the $TFSI^-$ and Pb^{2+}-$TFSI^-$ components. It then gradually reacts

with the released PbI_2 in a controlled reaction, leading to the formation of larger perovskite grains as illustrated in **Fig. 4b**. In contrast, without the addition of $TFSI^-$, the reaction proceeds rapidly between PbI_2 and FAI, resulting in the faster formation of smaller perovskite grains. Notably, owing to the hydrophobic nature of the $TFSI^-$, it can interact with the intermediate phases during crystallization (**Fig. S27, S28)**. This prevents uncontrolled dendritic growth and promotes the formation of uniformly dispersed crystals (**Fig. S29**). This delayed but superior crystallization process was also confirmed by excitation-emission matrix (EEM) fluorescence spectroscopy (**Fig. 4c, Fig. S30, S31**), which showed a delayed photoluminescence (PL) signal after annealing for 1 min compared to the pristine but with a significantly stronger intensity for the final KTFSI-PVSK sample, indicating fewer defects in the perovskite film.

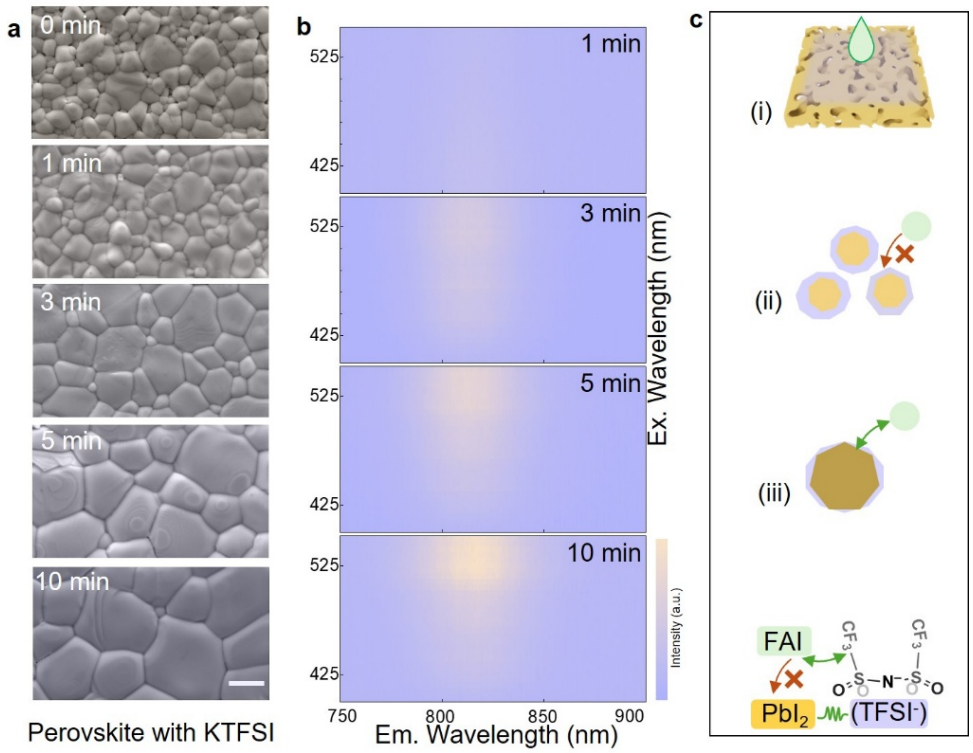

Fig. R3. a, SEM images tracking the morphological evolution of a KTFSI-doped perovskite film during the two-step crystallization process within 10 min. Scale bar: 1 μm. **b,** Three-dimensional excitation-emission matrix (EEM) fluorescence spectra of a KTFSI-doped perovskite film during different annealing times, mapping the PL intensity evolution in the 750-900 nm emission range under excitation from 400-500 nm. **c,** Schematic illustration of the proposed mechanism for KTFSI mediated perovskite grain growth. (i) FAI solution is added to the porous, KTFSI-incorporated PbI_2 layer. (ii) The resulting perovskite intermediate phase, surrounded by the $TFSI^-$ anions, is inhibited from further reacting with FAI. (iii) Upon heating, FAI overcomes the binding energy of the $TFSI^-$ coordination and reacts with the PbI_2, leading to

the formation of larger perovskite grains. Green squares and circles: FAI; Violet squares and polygons: $TFSI^-$ ions; Yellow substrate and polygons: PbI_2 and the unreacted perovskite intermediate phase.

2#5. The doped Spiro-OMeTAD exhibits a relatively low glass transition temperature, which limits the thermal stability of perovskite solar cells. The authors should conduct relevant stability assessments and include a dedicated discussion on this aspect.

Reply5:

Thank you for the important suggestions. We have supplemented the manuscript with the relevant experiments. The glass transition temperatures (T_g) of spiro-HTL films with different dopant compositions were measured using differential scanning calorimetry (DSC).

We investigated the effect of *t*BP concentration on the T_g of the NH_4TFSI-doped spiro-HTL. We found that the T_g decreases with increasing the *t*BP:THF ratio. The optimal *t*BP:THF = 1:1 ratio yields a T_g of 92 °C (**Fig. 3d, Fig. S15**). For the final co-doped strategy with OATFSI, the T_g is 90 °C (**Fig. S57**). This slight reduction is likely due to the plasticizing effect of OATFSI, which is an ionic liquid. We observed a similar, more pronounced reduction in T_g (to 80.3 °C) for spiro doped with another ionic liquid-like salt, DMATFSI. Importantly, the T_g of our optimized LODT-HTL (90 °C) is significantly higher than that of the conventional LiTFSI-spiro HTL (80.1 °C). This enhanced thermal robustness is reflected in the film's morphological stability.

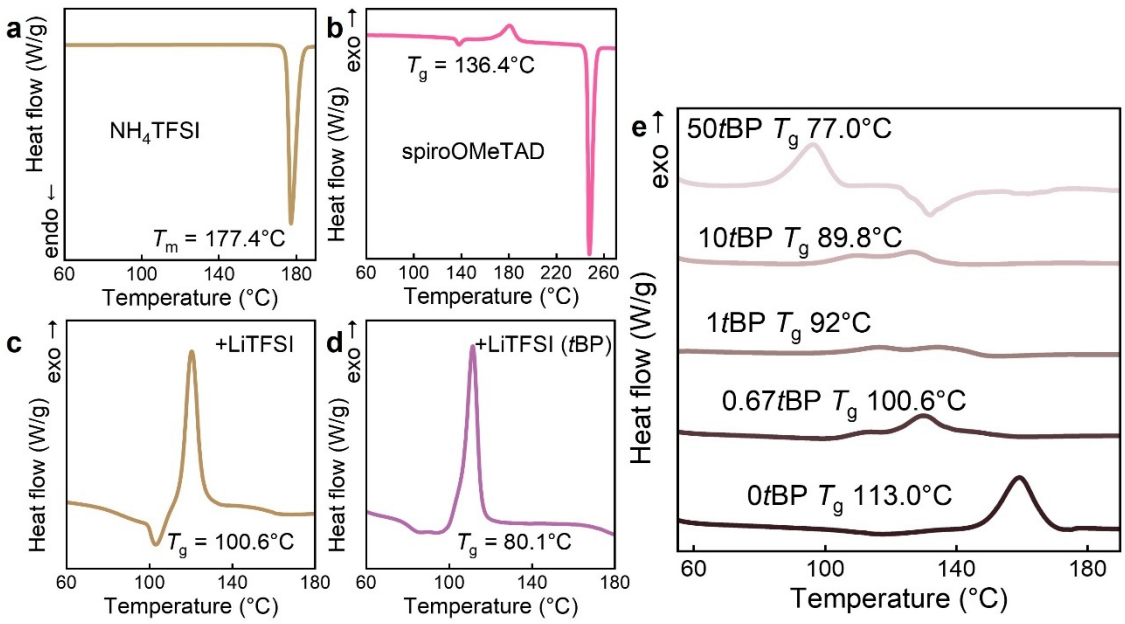

Fig. S15. Determination of glass transition temperature (T_g) by differential scanning calorimetry (DSC). a-d, DSC for **a,** pure NH_4TFSI, **b,** pristine spiro-OMeTAD, **c,** spiro-OMeTAD doped with LiTFSI, and **d,** spiro-OMeTAD doped with both LiTFSI and *t*BP in conventional HTL. **e,** DSC showing the changes in T_g for the NH_4TFSI-doped LODT-HTL as a function of *t*BP concentration.

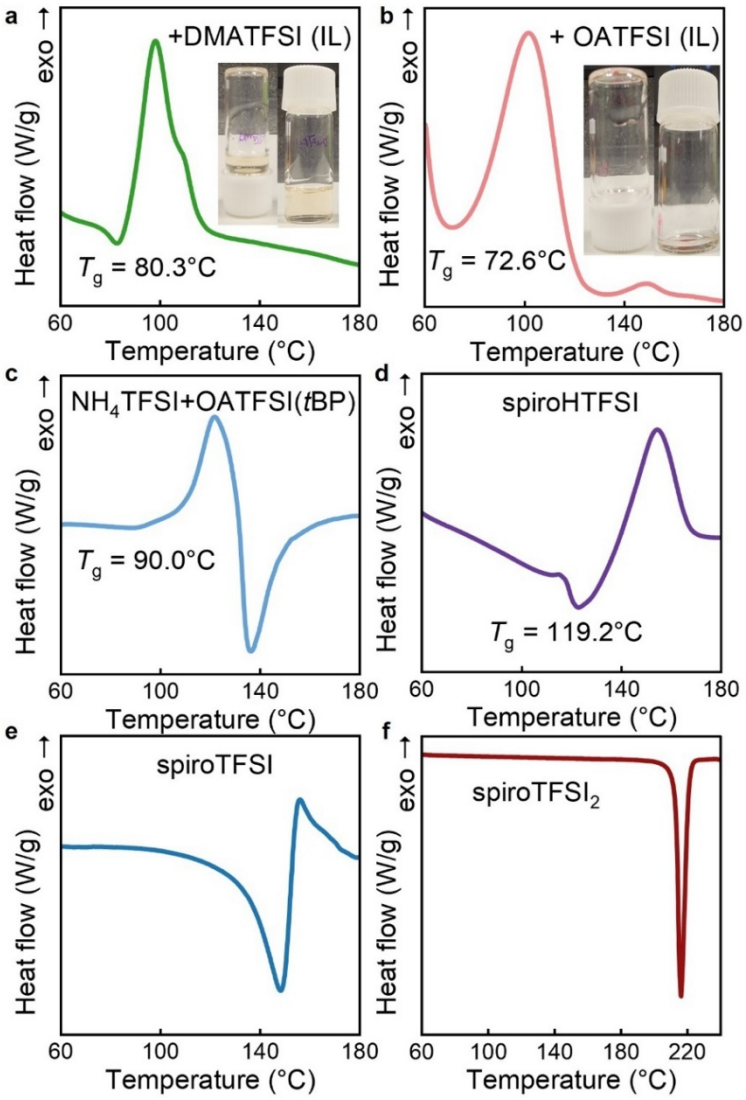

Fig. S57. DSC of spiro with various dopants. a, DMATFSI-doped LODT-HTL (T_g = 80.3 °C). The inset shows a photo of liquid DMATFSI. **b,** 100% mol OATFSI-doped LODT-HTL (T_g = 72.6 °C). The inset shows a photo of viscous, oily OATFSI; IL = ionic liquid. **c,** LODT-processed spiro co-doped with NH_4TFSI and 1% mol OATFSI (T_g = 90 °C). **d,** spiro doped with HTFSI (T_g = 119.2 °C). **e,** spiroTFSI, which shows no distinct glass transition. **f,** spiro$(TFSI)_2$, which shows no distinct glass transition or crystallization-induced exothermic features.

2#6. In line 341, the authors claimed "Furthermore, we found that OATFSI could also be employed in our LODT method by co-mixing with NH4TFSI.", it seems that no more details were provided for confirm this point.

Reply6:

Thank you for raising the above point. We deeply apologize for the missing part from the manuscript. Here we supplement the missing description of OATFSI co-doped with NH_4TFSI in LODT-HTL. The related content can be found on Page 14, lines 368-377 in the revised manuscript:

Furthermore, we found that OATFSI functions effectively as a dopant in the LODT-HTL (**Fig. S54**) and as a co-dopant with NH_4TFSI (**Fig. 5a**), yielding a high conductivity of 3.625×10^{-3} S/cm (**Fig. S55**). DAS analysis showed that the addition of OATFSI enhanced photo-excitation process of HTL, reducing the time from 29.6 ps to 21.3 ps corresponding to the NH_4TFSI only HTL (**Fig. S56, Fig. S10**). The improvement benefits hole extraction at the device interface compared with LiTFSI-spiro as confirmed by TRPL (**Fig. 5b, Fig. S40, Table S6**). However, its ionic liquid properties can lower the T_g of HTL (72.6 °C), compromising its thermal stability (**Fig. S57**). By choosing a minimal amount of OATFSI (1% mol to spiro), maintain a T_g of 90 °C while still improving conductivity (**Fig. S55**).

2#7. Given that the spiro-OMeTAD HTL was deposited via spin-coating—a technique with limited scalability—have the authors explored scalable deposition methods (e.g., blade-coating or slot-die coating) to validate the generalizability of their proposed mechanism for industrial-scale fabrication? Such validation would strengthen the practical relevance of this work.

Reply7:

Thank you for the valuable suggestions. To validate the scalability of our approach, we have performed additional experiments investigating the deposition of the LODT-HTL using a blade-coating (D-bar coating) process. By optimizing the coating parameters, such as the gap between the blade and the substrate (**Fig. S64a**), we controlled the HTL thickness to be comparable to that of our spin-coated films (~250 nm). We evaluated the uniformity of the resulting films and found that the thickness was consistent across multiple points on a 5 cm × 5 cm PSM (**Fig. S64c**). This successfully demonstrates the compatibility of our LODT-HTL with large-area deposition techniques, and we have also verified its applicability for fabricating 10 cm × 10 cm modules. The performance of the champion devices fabricated using this scalable method is comparable to that of our spin-coated devices, with the results summarized in **Table S9**.

Related description has been incorporated in the revised manuscript on Page 15, lines 398-402:

To extend the application of the LODT method to scalable blade-coating processes (D-bar coating), we optimized the relevant coating parameters. This enabled the deposition of highly uniform HTL films,

resulting in devices achieving champion PSM performance comparable to the spin-coated method (**Fig. S64, S65, Table S9**).

Table S9. Photovoltaic parameters of champion devices.

Champion Devices	Scan	V_{OC} (V)	J_{SC} (mA/cm^2)	FF (%)	PCE (%)	PCE H_{index} (RS/FS)
25 cm^2 PSM (D-bar coating)	RS	9.18	2.82	74.5	19.3	1.021
	FS	9.17	2.83	73.0	18.9	
100 cm^2 PSM (D-bar coating)	RS	18.20	1.13	51.5	12.15	1.038
	FS	17.73	1.17	50.6	11.7	

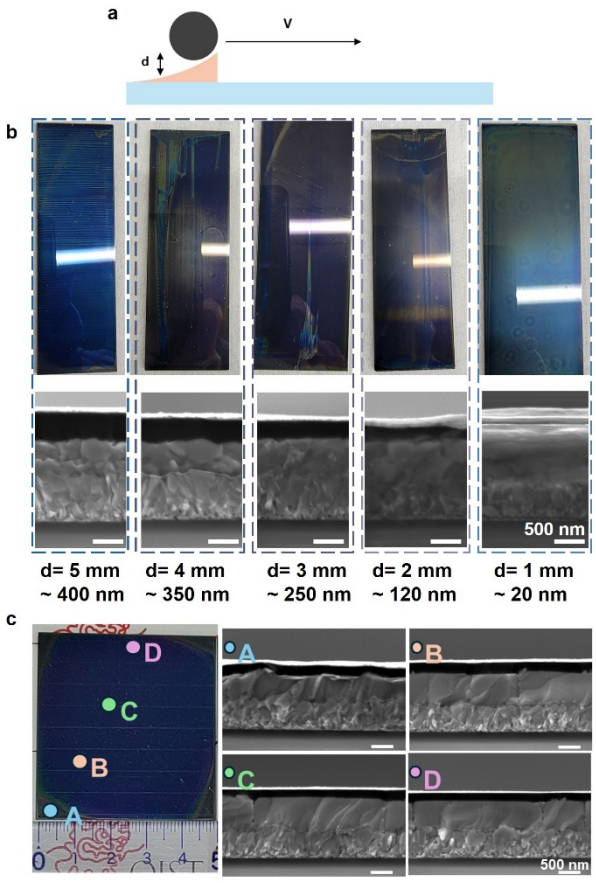

Fig. S64. Control of LODT-HTL layer thickness using D-bar coating. a, Schematic of the D-bar coating deposition process. The film thickness is controlled by varying the gap distance (*d*) between the blade and

the substrate, while the coating speed (*V*) is kept constant at 12 mm/s. **b,** Optical photographs (top row) and cross-sectional SEM images (bottom row) showing the spiro film thickness as a function of *d*. A gap of 2 mm yields a thickness of ~250 nm, comparable to that from spin-coating (240 nm). **c,** Uniformity assessment of the D-bar coated HTL. Cross-sectional SEM images taken at different points (A, B, C, D) on a 5 cm × 5 cm substrate demonstrate similar film thicknesses. The color variation at the corners of the PSM originates from thickness inhomogeneity caused by the two-step spin-coating deposition of the perovskite layer.

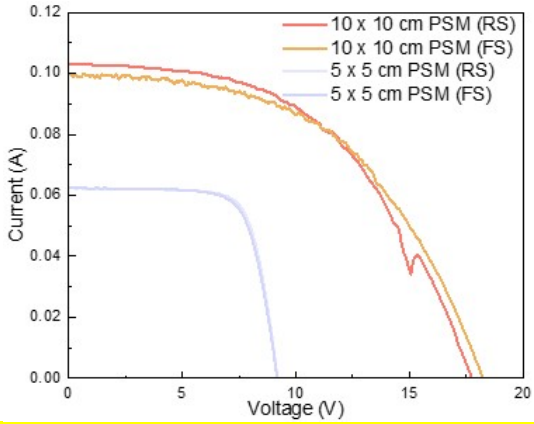

Fig. S65. *J-V* curves of the champion devices fabricated *via* D-bar coated PSM. *J-V* characteristics under reverse (RS) and forward (FS) scans for the champion PSM fabricated on 5×5 cm^2 and 10×10 cm^2 substrates, where the HTL was deposited by the D-bar coating method. The aperture areas are 22.08 cm^2 and 82.8 cm^2 for the 5×5 cm^2 and 10×10 cm^2 substrates, respectively.

2#8. The absence of aperture masks during mini-module certification raises concerns about potential overestimation of performance metrics. Moreover, the observed PCE discrepancy between forward/reverse scans suggests significant hysteresis—a behavior inconsistent with the significantly reduced hysteresis characteristics reported for small-area devices.

Reply8:

We are sorry for these missing details of the related description of certified PSM condition. The aperture area during certification is defined by the P4 design of PSM fabrication following previous work: 10.1016/j.joule.2024.06.026. As shown in **Fig. R4a**. The certified device was measured using the edge definition rather than a physical aperture mask. The P4, which is perpendicular to the sub-cells at the module edge, was used to separate the active central area from the inactive edge region. The purpose of this P4 is to accurately define the active area and to prevent short-circuiting from residual electrode material at the edges.

The revised contents were incorporated in the revised **supplementary information** on Page 6, line 159 to Page 6, line 167 and captions of **Fig. S63**:

The PSM shares the same fabrication process (two-step method) as the small area PSC, both applied for two-step FA-perovskite and $CsPbI_3$. The only difference is the additional laser processing to connect each sub-cell in series into an integrated PSM. For 5×5 cm^2 PSM, the P1 is designed with a width of 150 μm. After the deposition of ETL, perovskite and HTL, P2 pattern was conducted by laser scribing via a picosecond laser (Picosecond Laser Processing System, LPS-R002A, Spectronix Corporation), to remove layers above FTO. The P3 pattern was defined after gold deposition by similar laser cutting process to remove gold and separate each sub-cell. The P4 is used when no shadow mask is applied during test.

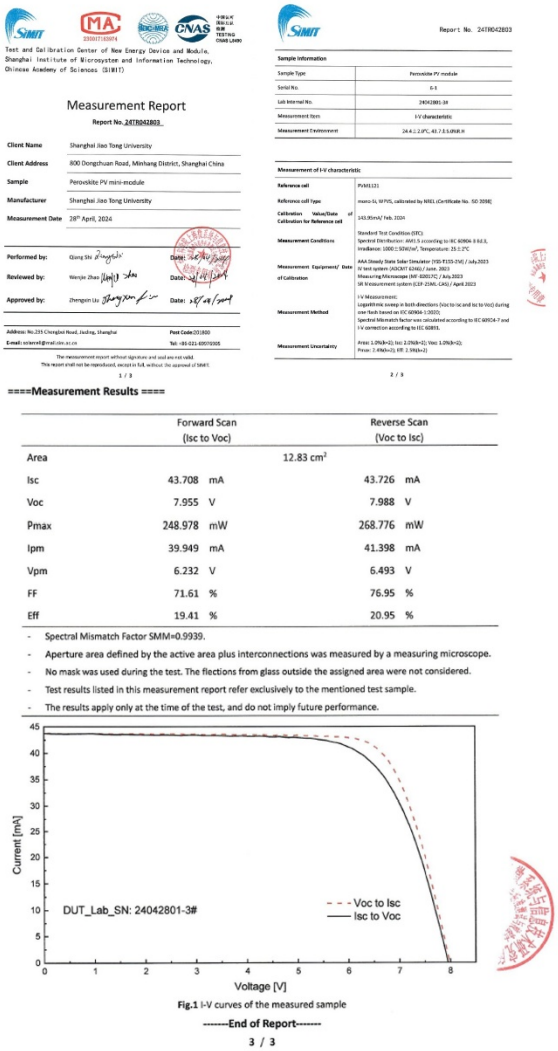

Test and Calibration Center of New Energy Device and Module,
Shanghai Institute of Microsystem and Information Technology,
Chinese Academy of Sciences (SIMIT)

Measurement Report

Report No. 24TR042803

Client Name	Shanghai Jiao Tong University
Client Address	800 Dongchuan Road, Minhang District, Shanghai China
Sample	Perovskite PV mini-module
Manufacturer	Shanghai Jiao Tong University
Measurement Date	28th April, 2024

Performed by: Qiang Shi Date:
Reviewed by: Wenjie Zhao Date:
Approved by: Zhengxin Liu Date:

Address: No.235 Chengbei Road, Jiading, Shanghai Post Code:201800
E-mail: sciservice@mail.sim.ac.cn Tel: +86-021-69979906

The measurement report without signature and seal are not valid.
This report shall not be reproduced, except in full, without the approval of SIMIT.

1 / 3

Report No. 24TR042803

Sample Information

Sample Type	Perovskite PV module
Serial No.	6-5
Lab Internal No.	24042801-3#
Measurement Item	I-V characteristic
Measurement Environment	24.4 ± 2.3°C, 41.7 ± 5.6%R.H

Measurement of I-V characteristic

Reference cell	PVM121
Reference cell Type	mono-Si, WPVS, calibrated by NREL (Certificate No. ISO 2036)
Calibration Value/Date of Calibration for Reference cell	143.95mA/ Feb. 2024
Measurement Conditions	Standard Test Condition (STC) Spectral Distribution: AM1.5 according to IEC 60904-3 Ed.3, Irradiance: 1000 ± 30W/m², Temperature: 25 ± 2°C
Measurement Equipment/ Date of Calibration	AAA Steady State Solar Simulator (YSS-T155-2SE) / July.2023 IV test system (ADCIVT 6266) / June. 2023 Measuring Microscope (MF-A2012C) / July.2023 SR Measurement system (CEP-25MS-CAS) / April.2023
Measurement Method	I-V Measurement: Logarithmic sweep in both directions (Voc to Isc and Isc to Voc) during one flash based on IEC 60904-1:2020; Spectral Mismatch factor was calculated according to IEC 60904-7 and I-V correction according to IEC 60891.
Measurement Uncertainty	Area: 1.0%(k=2); Isc: 2.0%(k=2); Voc: 1.0%(k=2); Pmax: 2.4%(k=2); Eff: 2.5%(k=2)

2 / 3

====Measurement Results ====

	Forward Scan (Isc to Voc)		Reverse Scan (Voc to Isc)	
Area	12.83 cm^2			
Isc	43.708	mA	43.726	mA
Voc	7.955	V	7.988	V
Pmax	248.978	mW	268.776	mW
Ipm	39.949	mA	41.398	mA
Vpm	6.232	V	6.493	V
FF	71.61	%	76.95	%
Eff	19.41	%	20.95	%

- Spectral Mismatch Factor SMM=0.9939.
- Aperture area defined by the active area plus interconnections was measured by a measuring microscope.
- No mask was used during the test. The flections from glass outside the assigned area were not considered.
- Test results listed in this measurement report refer exclusively to the mentioned test sample.
- The results apply only at the time of the test, and do not imply future performance.

Fig.1 I-V curves of the measured sample

--------End of Report--------

3 / 3

Fig. S63. The certification report of PSM on 12.83 cm^2 issued from a third-party independent certification center [Shanghai Institute of Microsystem and Information Technology (SIMIT)]. Note: No mask was used

for test, the aperture area is defined by the active area with P1 and P4 plus interconnections measured by an optical microscope.

We have also revised **Fig. S62** providing detailed description of P4 design for PSM fabrication.

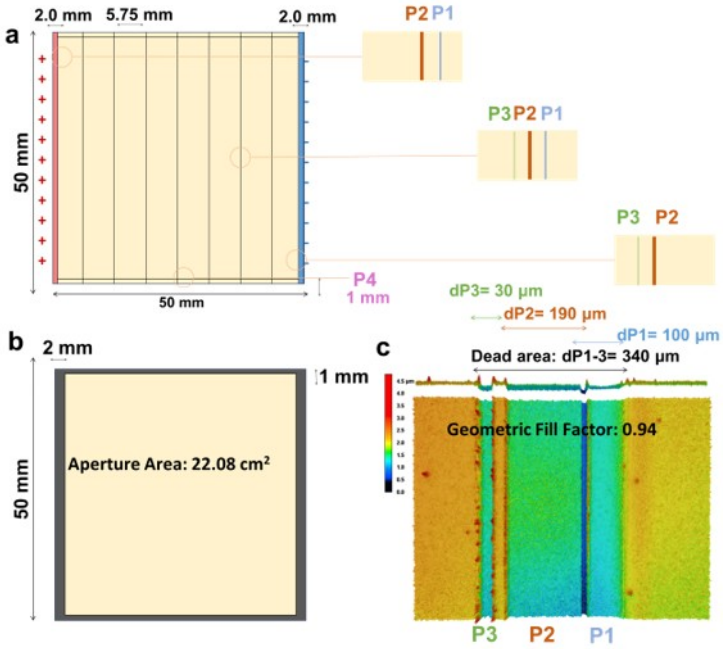

Fig. S62. Design, layout, and characterization of the 5 cm × 5 cm PSM. a, Schematic of the PSM layout on a 5 cm × 5 cm substrate. The positive and negative electrodes are 2 mm wide, each sub-cell has a width of 5.75 mm, and a 1 mm wide P4 scribe is used for edge isolation after Au deposition. **b,** Diagram of the aperture mask used for device characterization. The frame dimensions correspond to the electrode and P4 scribe widths, defining a final aperture area of 22.08 cm². **c,** 3D pseudo-color image from laser scanning microscopy used to determine the dimensions of the P1, P2, and P3 scribe lines, with color representing surface topography. The total interconnect distance (P1 to P3) is 340 µm, resulting in a calculated geometric fill factor (GFF) of approximately 0.94.

Regarding the second point of Reviewer's concern regarding hysteresis, we have evaluated the efficiency measurements of PSM using a black-painted aperture mask with a defined area of approximately 22 cm^2. The statistical data of PSM performances were incorporated in **Fig. S61b** and **Table S10**. We note that for the PSMs, the hysteresis index (H_{index}) is slightly larger compared to the small-area PSCs. We attribute this to the P2, P3, and P4 laser scribing processes, which are performed in ambient air with relatively high humidity. After the P2 scribe, the edge of each sub-cell is fully exposed to air, which can lead to direct decomposition of the bulk perovskite and thus cause hysteresis. For the certified device, the reverse scan PCE was 20.95% and the forward scan PCE was 19.41%, giving an H_{index} of 1.079. This is close to the

average H_{index} of 1.054 that we obtained in our lab. The certified device was unencapsulated, and under the ambient humidity of the testing facility, degradation may have occurred primarily along the channel near the P3 scribe. This could cause the formation of residual lead iodide, leading to a slight increase in hysteresis compared to our lab measurement.

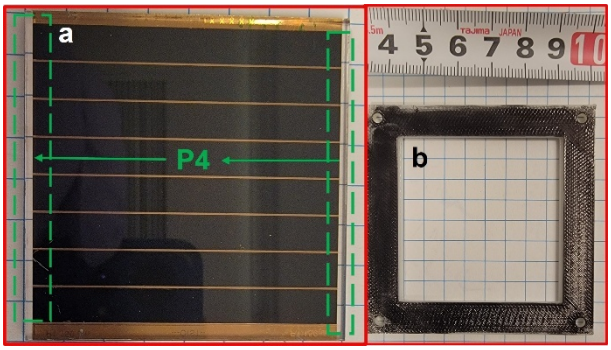

Fig. R4a, Photo of devices with cleaned edge (in green box) by P4 in lab. **b,** Shadow mask for PSM test in lab with painted by black color.

Table S10. Summary of statistical data of photovoltaic parameters from PSC and PSM devices.

Device	Condition	Scan	V_{OC} (V)	J_{SC} (mA/cm^2)	FF (%)	PCE (%)	PCE H_{index} (RS/FS)
PSC	Target	RS	1.18±0.01	23.63±0.75	79.7±2.44	21.85±0.89	1.017
		FS	1.18±0.01	23.63±0.76	79.67±2.42	21.42±0.83	
	Control	RS	1.07±0.02	23.35±0.74	73.9±4.96	18.75±1.03	1.383
		FS	1.07±0.04	23.36±0.61	52.9±6.15	13.55±1.49	
PSM	Target	RS	9.06±0.44	2.83±0.12	72.6±4.15	18.62±1.54	1.054
		FS	8.96±0.40	2.81±0.093	70.2±3.73	17.65±1.17	
	Control	RS	8.51±0.41	2.82±0.17	67.8±3.02	16.76±0.68	1.558
		FS	8.48±0.59	2.81±0.16	45.59±2.85	10.76±0.48	

We thank you once again for your detailed questions and guidance on our work, which prompted us to conduct a more thorough investigation into the role of *t*BP within the LODT process and the mechanism of TFSI-regulated perovskite growth. This has led us to a much deeper understanding of the conditions and the underlying reasons for the LODT-HTL working mechanism. Through a multi-faceted investigation into KTFSI's role, combined with insights from prior literatures, we were able to propose a plausible mechanism for how TFSI regulates perovskite crystallization. This understanding is critical for successfully implementing TFSI additives as a comprehensive tool to enhance both device stability and efficiency. Especially, we thank you for inspiring us to explore the broader applicability of the LODT method. This has provided valuable experience and data that supports its potential for future large-scale, industrial-level implementation.

Response to Reviewer #3

Zhang et al. reports a lithium-free and air-free oxidation of spiro-OMeTAD using a combination of organic ammonium TFSI salts and UV light. In addition to spiro-OMeTAD oxidation, other TFSI salts are also investigated for 3D perovskite doping and interface passivation: (1) potassium TFSI is added to the 3D perovskite to improve crystallisation and grain size, and (2) octylammonium TFSI is used to form a 2D/3D perovskite passivation layer. The authors then fabricated small area and mini-module solar cells with improved efficiency. However, lithium-free oxidation, air-free oxidation, and UV-assisted oxidation of spiro-OMeTAD have all been reported many times before. For example doi.org/10.1126/science.abo2757, doi.org/10.1002/aenm.201901519, doi.org/10.1038/s41467-024-52199-4, 10.1016/j.joule.2024.03.012, doi.org/10.1021/acsaem.4c01314. The use of potassium and octylammonium salts are also very common in the literature. This manuscript presents no new insights that have not been reported before in previous literature. In addition, the solar cell results here are not competitive with current standards in the literature, especially compared to the inverted pin devices that are efficient and stable even at high temperatures (85°C). This reviewer also has further technical concerns regarding the authors' claims below.

Reply:

Thank you for raising the important points regarding the novelty of our work. Indeed, lithium-free, oxygen-free, and light-assisted oxidation of spiro-OMeTAD have been individually reported. However, the novelty of our study lies in the holistic and systematic decoupling of the roles of both the cation and the anion in versatile TFSI salts, and their cooperative use across different layers of the device architecture.

Specifically, **(i)** we demonstrate for the first time that NH_4TFSI can accelerate the light-induced oxidation of spiro-OMeTAD in solution through proton-coupled electron transfer, leading to faster and more efficient doping than previously reported photo-oxidation processes; **(ii)** we reveal the direct role of $TFSI^-$ anions in modulating perovskite crystallization and energetics by incorporating KTFSI in the precursor solution; **(iii)** we employ OATFSI to create a thermally robust 2D/3D interface with enhanced hydrophobicity. Importantly, we integrate these synergistic functions in a holistic strategy that enables both high efficiency and stability and demonstrate its scalability to 5 × 5 cm^2 PSMs.

Furthermore, in the revised manuscript, we have added new data on the operational stability of our devices at elevated temperatures, as shown in **Fig. S66**. For encapsulated small-area cells, we achieved a T_{90} lifetime of 491 hours under continuous operation at 45 °C. Notably, our PSMs also demonstrated significantly improved stability at 45 °C compared to the control group, reaching a T_{80} lifetime of 375 hours. Even at a higher temperature of 65 °C, although an initial drop in efficiency was observed in the first 100 hours, the module's performance stabilized at 75% of its initial value and remained stable for about 500 hours. To the

best of our knowledge, this represents the outstanding high-temperature operational stabilities reported for large-area n-i-p modules under continuous illumination.

More than that, we demonstrate the versatility and robustness of the LODT-HTL based on the **(i)** scalability, demonstrating the compatibility with blade-coating (**Fig. S64**), and **(ii)** generality, where the LODT-HTL method was also applied to fabricate inorganic $CsPbI_3$-based PSMs, achieving both competitive efficiency and exceptional high-temperature stability, with a T_{89} lifetime of 571 hours at 65 °C. We attribute these significant enhancements in stability and versatility to the simplified additive strategy of the LODT method, which results in a spiro-HTL with a significantly elevated glass transition temperature and stable morphologies under heat (**Fig. S67**).

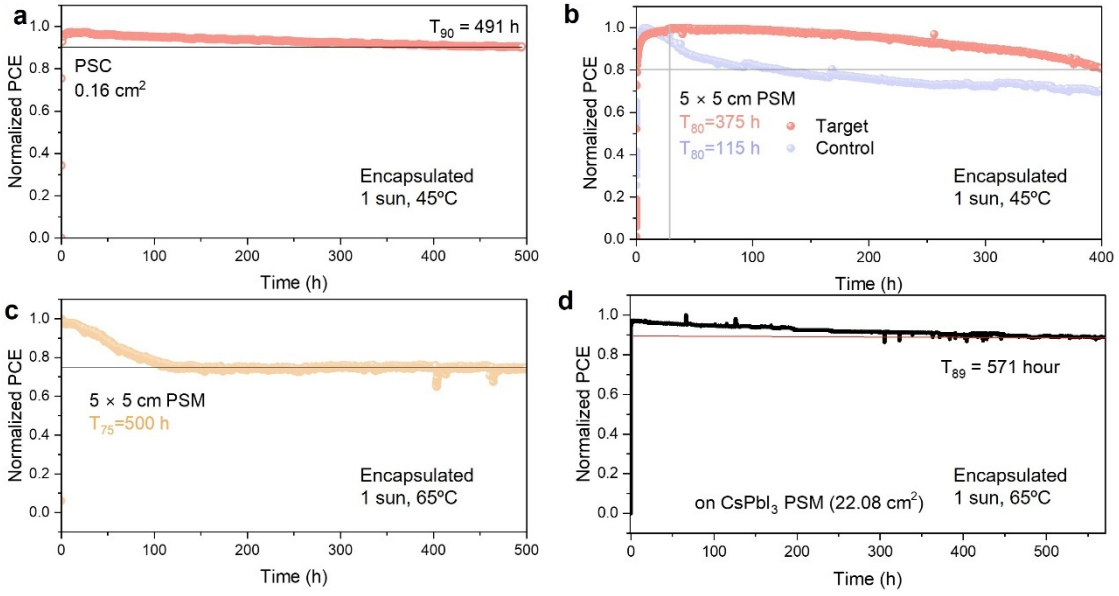

Fig. S66. Thermal stability of perovskite solar cells and module. a, Higher temperature stability of a small-area PSC (encapsulated by UV glue with top glass) under continuous 1-sun illumination at 45 °C. The T_{90} lifetime is 491 hours. **b,** Thermal stability comparison of PSM, control and target from the holistic strategy, tested at 45 °C. The T_{80} lifetimes are 375 hours and 115 hours for the target and control devices, respectively. **c,** Thermal stability of PSM under 65 °C with encapsulation. With T_{75} of 500 hours. **d,** Thermal stability of an encapsulated inorganic $CsPbI_3$-based PSM employing the LODT-HTL, tested at 65 °C. The device exhibits a T_{89} lifetime of 571 hours.

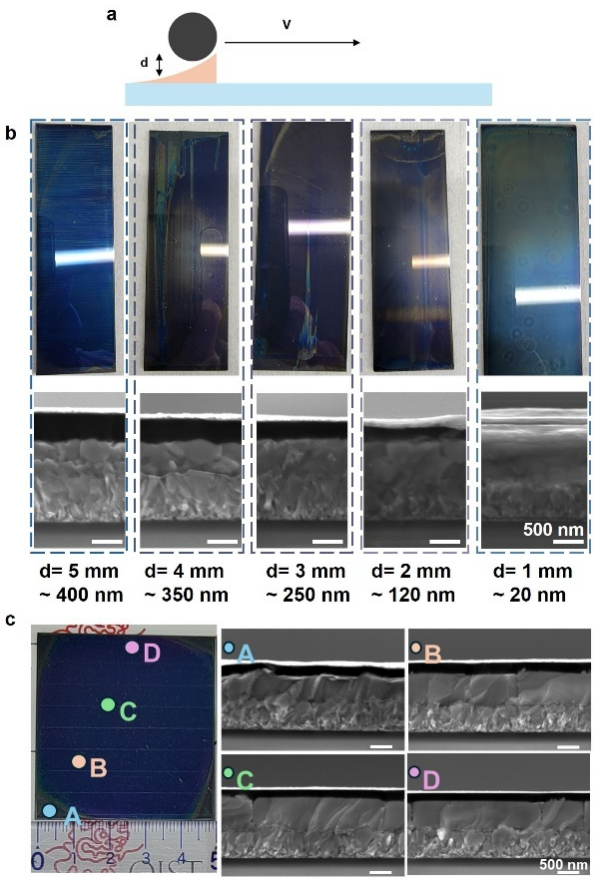

Fig. S64. Control of LODT-HTL layer thickness using D-bar coating. a, Schematic of the D-bar coating deposition process. The film thickness is controlled by varying the gap distance (*d*) between the blade and the substrate, while the coating speed (*V*) is kept constant at 12 mm/s. **b,** Optical photographs (top row) and cross-sectional SEM images (bottom row) showing the spiro film thickness as a function of *d*. A gap of 2 mm yields a thickness of ~250 nm, comparable to that from spin-coating (240 nm). **c,** Uniformity assessment of the D-bar coated HTL. Cross-sectional SEM images taken at different points (A, B, C, D) on a 5 cm × 5 cm substrate demonstrate similar film thicknesses. The color variation at the corners of the PSM originates from thickness inhomogeneity caused by the two-step spin-coating deposition of the perovskite layer.

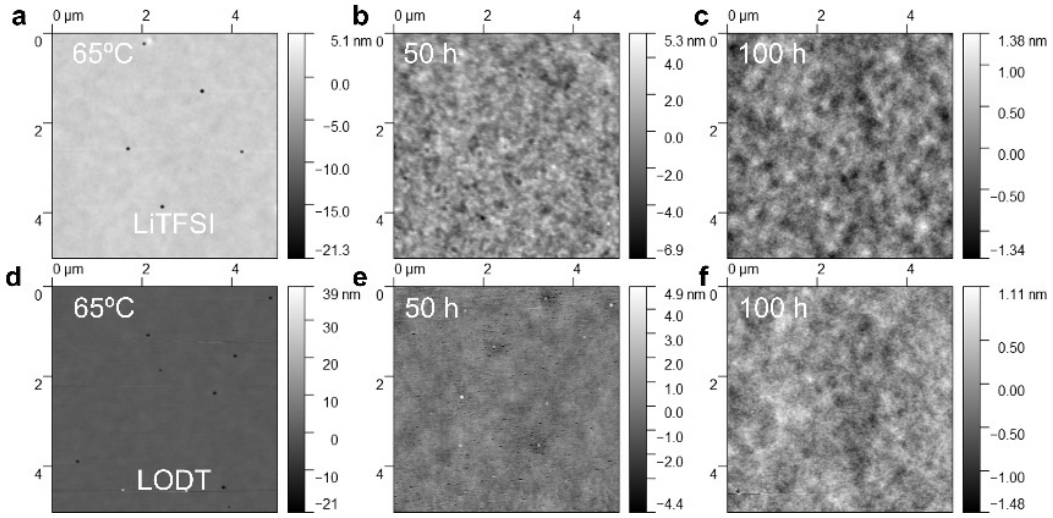

Fig. S67. Morphological evolution of LiTFSI-spiro and LODT-HTL films during thermal aging at 65 °C in air. a,b,c Surface morphology of the LiTFSI-spiro film **a,** before, **b,** after 50 hours annealing and **c,** after 100 hours annealing in air at 65 °C. The aged film exhibits notable aggregation. **d,e,f,** Surface morphology of the LODT-HTL **d,** before, **e,** after 50 hours annealing and **f,** after 100 hours annealing in air at 65 °C, showing no significant aggregation of films. Formation of pinholes on the fresh LiTFSI-spiro films have been previously reported.[S4]

3#1 UV light above the bandgap of spiro (>3.2eV) is required for photo-oxidisation. Yet, the authors claim that ambient light can trigger spiro photo-oxidisation. Since ambient light (LED or fluorescent) does not emit UV, so what is the UV source? The authors should provide a spectrum of their ambient light. In addition, how does the optical power and emission spectrum of UV affect the LODT spiro oxidation?

Reply1:

Thank you for your questions. We have supplemented the manuscript with the corresponding experiments and revised the relevant paragraphs to address the reviewer's valuable questions about the role of ambient light. In brief, we have systematically investigated the relationship between the wavelength and intensity of incident light and the rate of spiro-OMeTAD oxidation.

Response of different additives to white light: As shown in **Figures 2c, S5, S8, and S9**, we found that, with the exception of TeMATFSI, all proton-containing ATFSI salts can trigger the oxidation of spiro-OMeTAD under white light illumination. TeMATFSI is an exception because $(CH_3)_4N^+$ cannot release free protons. The effect was most pronounced with NH_4TFSI, which corresponds to the stronger acidity of the NH_4^+ cation and its ability to provide protons.

Effect of wavelength: We irradiated the NH_4TFSI spiro solution with various wavelengths (365, 450, 550, 650, and 850 nm). The results clearly show that the shorter the wavelength (i.e., the higher the photon energy), the faster the rate of oxidation. Notably, under 365 nm UV light (~3.4 eV), the absorbance reached saturation almost instantly. Compared to longer wavelengths, 450 nm light (~2.76 eV) was also very effective at promoting oxidation. This confirms that higher-energy photons more effectively accelerate the oxidation process, while 850 nm light induced almost no oxidation.

Mechanism explanation: This phenomenon can be explained by our proposed mechanism. First, NH_4TFSI releases protons in the solution, which are captured by the basic spiro-OMeTAD (spiro) molecule to form a spiro-HTFSI intermediate. Subsequently, when a photon excites a spiro molecule to its excited state (spiro*), an electron from spiro* is captured by H^+, forming an oxidized $spiro^+$ radical and causing the solution's color to change. Higher-energy photons can generate more spiro* molecules within a given time, thus accelerating the reaction, which is consistent with our observations on light intensity dependence shown in **Fig. S9.**

Role of ambient light: The reason that visible light, even at 550 nm or 650 nm, can still promote the reaction is explained by the properties of the excited state. According to our TAS measurements (**Fig. S10f**), the excited spiro* state has a broad absorption profile in the 400-700 nm range, with a strong absorption near 400 nm. Common white LEDs have a strong emission peak in the 400-800 nm range (**Fig. S2 b, c**). Therefore, even the visible light from an LED inside a glovebox contains a sufficient blue-light component (~400 nm) to excite spiro-OMeTAD and initiate the LODT phenomenon.

The above new contents and discussion were incorporated on Page 6, line 124 to Page 8, line 172 of the revised manuscript:

The light treatment process and proposed reaction are schematically shown in **Fig. 2a, b**. Control experiments ruled out solvent-induced doping and contributions from trace oxygen or moisture (both < 0.1 ppm, **Fig. S2, S3**). Using a home-built *in situ* UV-Vis-NIR setup inside N_2 glovebox, we monitored the absorbance changes over time under continuous illumination. The oxidized spiroTFSI and other related oxides displayed distinct absorption signatures compared to pristine spiro, most prominently in the near-infrared region (**Fig. S4**).[25] As anticipated, four of the ATFSIs (NH_4TFSI, MATFSI, DMATFSI, and TMATFSI) induced clear photo-responses, given by the increasing absorbance signals (**Fig. S5**), whereas TeMATFSI showed negligible effect because $(CH_3)_4N^+$ cannot release free protons. Notably, the oxidation ability varied across different cations as demonstrated in **Fig. 2c**. For example, within 4 min, NH_4TFSI and MATFSI resulted in a rapid absorbance growth at 1521 nm, significantly faster than DMATFSI. However,

TMATFSI with the lowest pK_a, expected to be the strongest oxidant, showed slow absorbance changes, likely due to its inadequate dissociation in THF.[38] After 4 min, NH_4TFSI exhibited a sudden growth in absorbance, which can be attributed to the release of NH_3 and thus more release of protons.[26] Upon THF evaporation in glovebox at room temperature, the resulting doped spiro solids retained the radicals features as confirmed by electron spin resonance (ESR) spectroscopy (**Fig. 2d**), consistent with the UV–Vis results. Ultraviolet photoelectron spectroscopy (UPS) further confirmed effective p-type doping and conductivity enhancement for most ATFSI except TeMATFSI (**Fig. S6, S7** and **Table S1**). Based on these results, NH_4TFSI was selected as the efficient additive for LODT-HTL.

To elucidate the role of light in the LODT process, we employed irradiation wavelengths of 365, 450, 550, 650, and 850 nm. Except 850 nm, the shorter wavelengths and stronger light powers lead to faster absorbance growth of spiro solutions(**Fig. S8, S9**). This result highlights the role of higher-energy photons in helping with acceleration in spiro oxidation process efficiently. As the doping mechanism of NH_4TFSI involves proton-coupled electron transfer[23] from the photoexcited spiro* to spiro$^+$, abundant and higher-energy photons (wavelength of 365 nm equivalent to 3.4 eV) are more efficient in populating the excited state of spiro*. In LODT, the reaction can be presented as: $spiro + NH_4TFSI \rightarrow spiroHTFSI + NH_3$ and light accelerates the reaction of $spiroHTFSI + spiro^* \xrightarrow{hv} spiro + spiro^{\cdot+}\ TFSI^- + {}^1/_2\, H_2$. Here, the photoexcited spiro* readily transfers an electron to the proton, following with the reduction of proton to hydrogen, thereby generating the oxidized radical (spiro$^+$ or spiro$^{\bullet+}$) easily under suitable light activation (**Supplementary Note S1**). The resulting spiro$^+$ is stabilized by the TFSI$^-$ anion, while the deprotonated spiro species remains in the system and can further participate in subsequent reactions. Collectively, above results demonstrate that light irradiation is an effective method of accelerating the NH_4TFSI-induced oxidation of spiro in solution. Then, we performed femtosecond transient absorption spectroscopy (TAS) to study the oxidation activation process under the light exposure. Pristine spiro-HTL exhibited a broad peak in the range of 420-550 nm (**Fig. S10f**). After doping with NH_4TFSI, an additional response emerged within 560-610 nm (**Fig. S10l**), characteristic of the excited state spiro* species.[36],[39] This indicates that pristine spiro, without TFSI$^-$, cannot efficiently undergo the excitation-induced oxidation (spiro* → spiro$^+$). Decay-associated spectra (DAS) further support that and the analysis with triple-exponential fitting revealed that LODT-HTL undergoes a distinct decay pathway leading to oxidized radical cations, indicated by a prominent 530 nm feature from spiroTFSI. In contrast, no similar signature was observed for the pristine spiro (**Fig. 2e, f**), suggesting the effective doping of spiro-HTL.

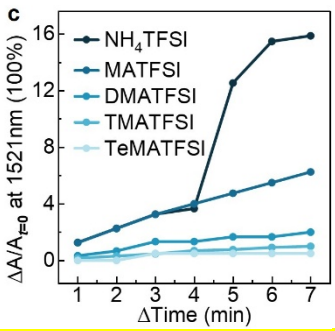

Fig. 2c, Time-resolved UV-Vis-NIR absorption monitoring of the spiro oxidation process with different ATFSIs under white-light LED illumination. The plot shows the percentage increase rate (ΔA) of absorbance (A) relative to the initial absorbance ($A_{t=0}$) at the peak of 1521 nm.

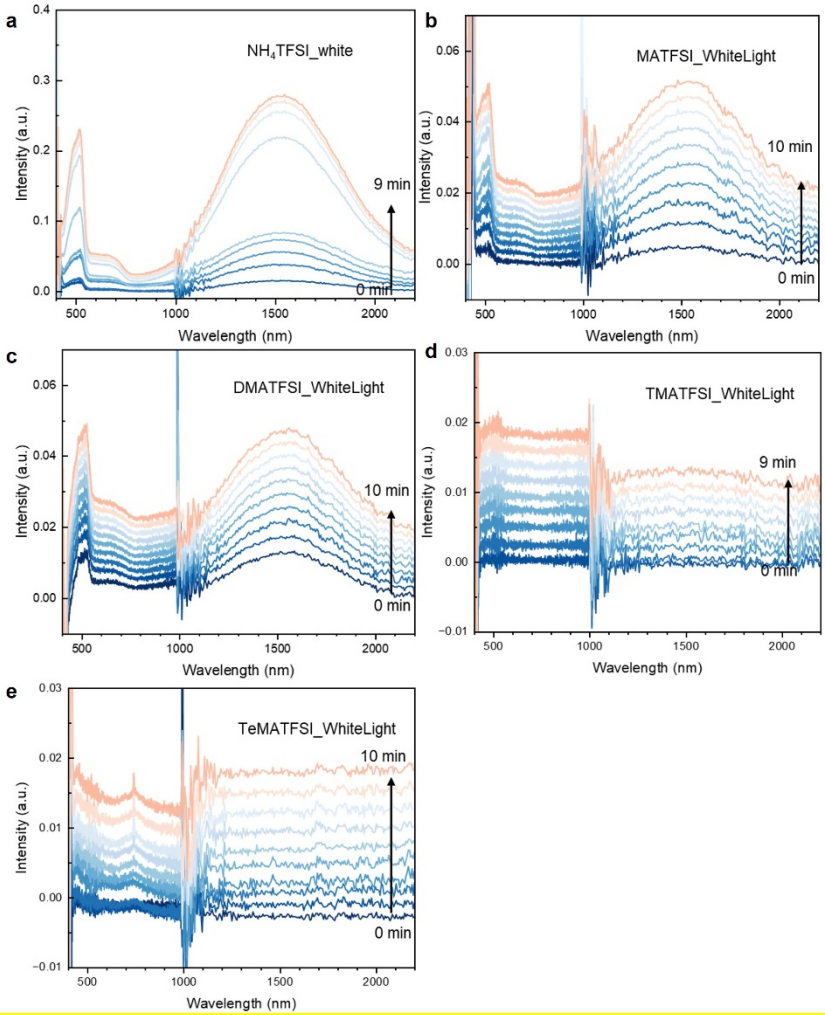

Fig. S5. Photoresponsivity absorption of spiro-OMeTAD solutions doped with various ATFSI salts. Time-resolved UV-Vis-NIR absorption spectra of spiro-OMeTAD solutions doped with **a,** NH_4TFSI, **b,** MATFSI, **c,** DMATFSI, **d,** TMATFSI, and **e,** TeMATFSI, measured under continuous white LED

illumination in 10 min. The sharp spikes are due to the influence of switching different light sources from instrument during test.

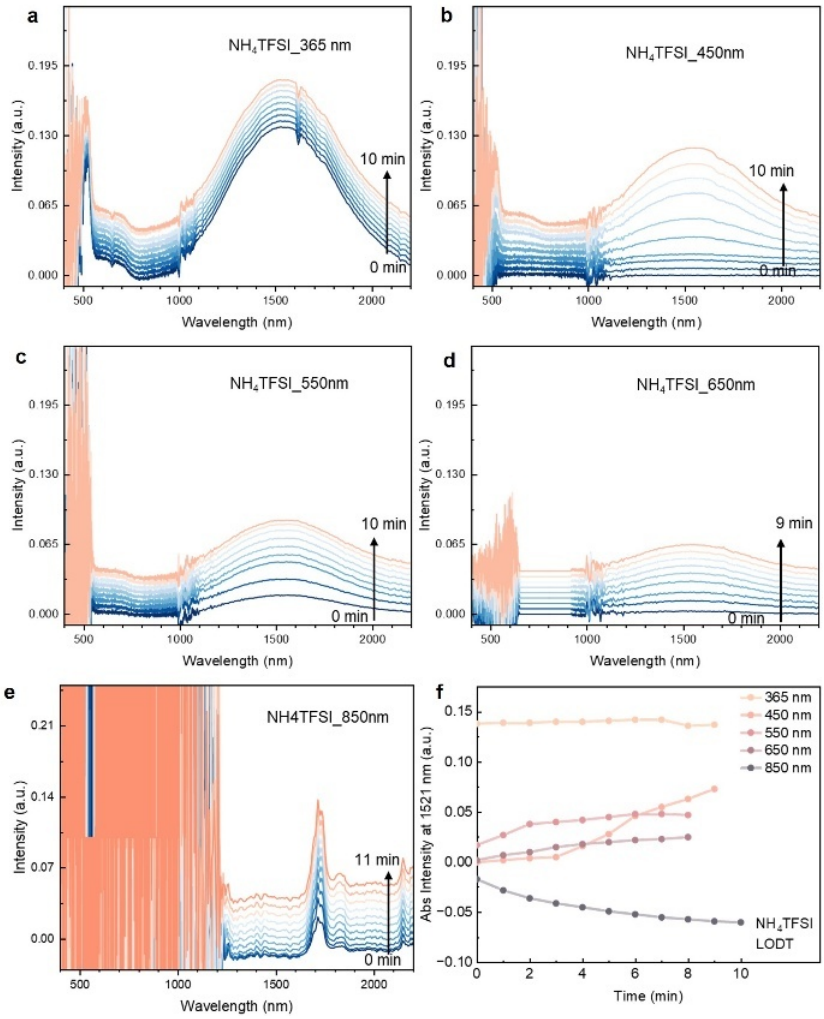

Fig. S8. UV-Vis-NIR spectra of NH_4TFSI-doped spiro-OMeTAD solution under illumination at different wavelengths. Evolution of the absorption spectra for an NH_4TFSI-doped spiro-OMeTAD solution in THF under monochromatic LED light source illumination. The illumination wavelengths for the respective panels correspond to **a,** 365 nm, **b,** 450 nm, **c,** 550 nm, **d,** 650 nm, and **e,** 850 nm. **f,** Absorbance intensity changes at 1521 nm under different light illumination. The sharp peak around 1700 nm in (**e**) can be attributed to the two low-lying transitions of $spiro^+$.[S2]

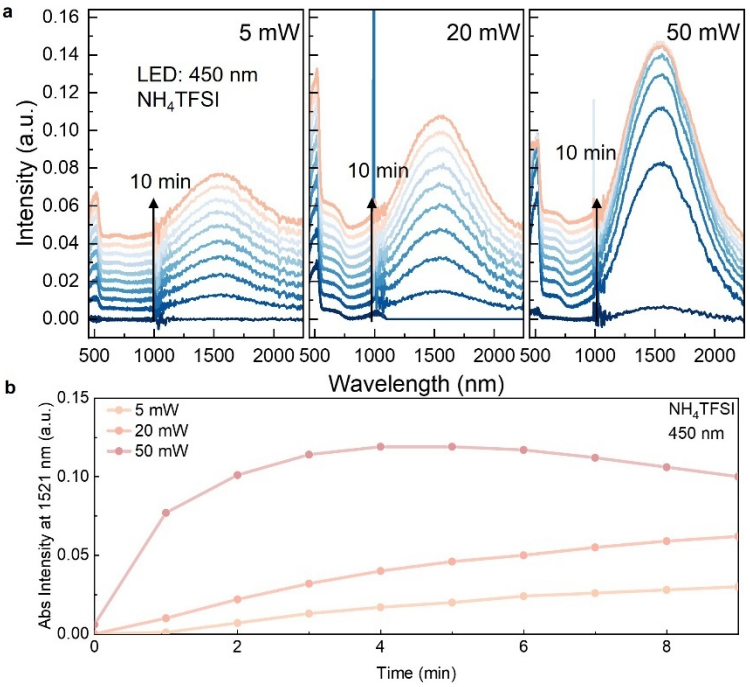

Fig. S9. Light intensity dependence of the LODT NH_4TFSI-doped spiro-OMeTAD. a, Absorbance changes of NH_4TFSI-doped spiro-OMeTAD solution over the same time period under illumination with a 450 nm LED at various power levels (5 mW, 20 mW and 50 mW) in 10 min. **b,** Absorbance intensity changes at 1521 nm illuminated by 450 nm *via* different power of light.

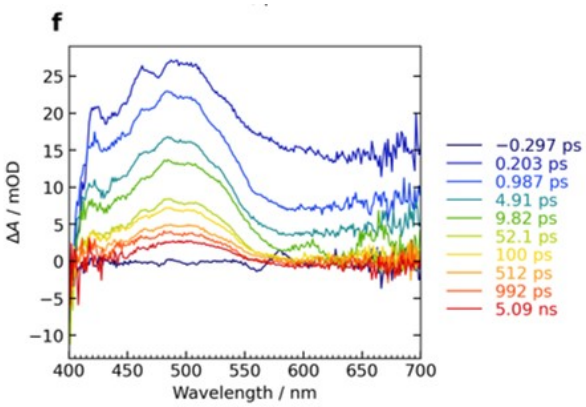

Fig. S10f Pump-probe transient absorption spectroscopy (TAS) of pristine spiro-HTL.

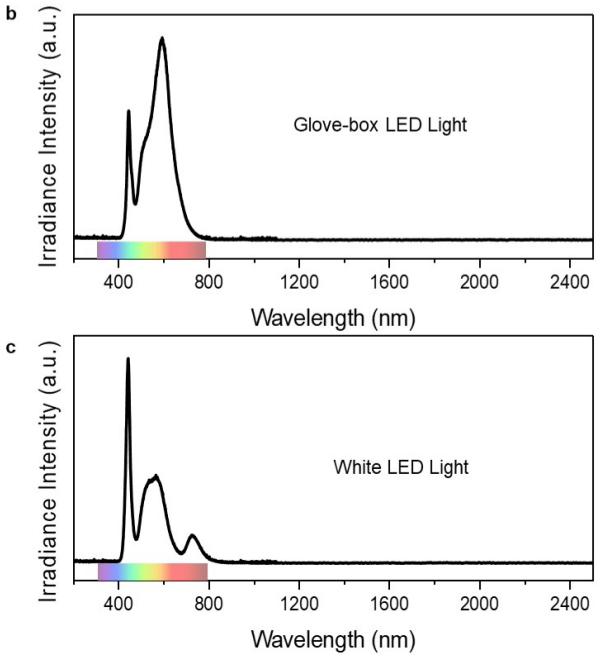

Fig. S2 b, Full-range emission spectrum of the LED lights used for general illumination within the glovebox. **c,** Emission spectrum of the white LED used for the LODT tests.

3#2 Related to above, 10 ppm O2/H2O is 2 orders magnitude higher than a standard glovebox (<0.1ppm). In this case, have the authors excluded O2/H2O contamination in the glovebox assisting with the spiro oxidation?

Reply2:

Thank you for your important question. We have carried out all the experiments in a new N_2-filled glovebox with an active purification system, where the moisture and O_2 levels were below 0.1 ppm (**Fig. S2a**).

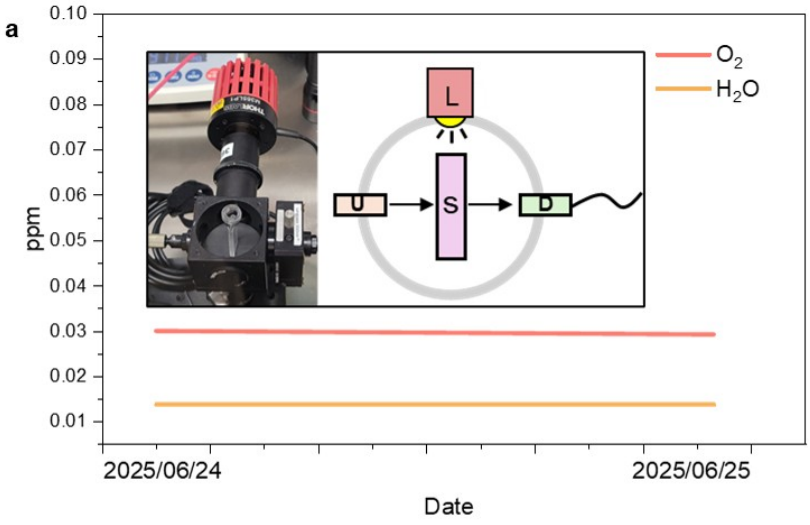

Fig. S2a. Setup and operating conditions for *in-situ* ultraviolet-visible-near-infrared (UV-Vis-NIR) absorption measurements. a, Variation of H_2O and O_2 concentrations inside the glovebox (< 0.1 ppm). The inset shows the custom-built *in-situ* UV-Vis-NIR measurement setup, where U is the spectrometer's light source with bandpass filter, D is the detector, S is the sample slot, and L is the external, variable-wavelength LED for sample illumination.

3#3 What is the role of tBP and THF in the LODT spiro? tBP-free and lithium-free spiro has already been demonstrated for pre-oxidised spiro (e.g. doi.org/10.1126/science.abo2757), so is tBP and THF still necessary? The experiments in Fig. S7 may not be relevant because tBP is diluted in the solvent (e.g. chlorobenzene) during spiro deposition on to the perovskite.

We thank the reviewer for the question. As also asked by Reviewer #2, we have supplemented the revised manuscript with additional experiments to clarify this point. The relevant description can be found in our response to comment #1 from Reviewer #2 (**Response letter** Page 23 to Page 29)

In brief, THF serves as a good common solvent for both ATFSI and spiro-OMeTAD, ensuring that the reaction between them is not disturbed by side reactions (such as complexation). THF promotes the solubility of ATFSI in the final chlorobenzene-based spiro solution, while the addition of *t*BP is primarily to improve the film-forming properties. However, our new experiments revealed a complex trade-off with *t*BP. We found that as *t*BP is added, it progressively de-dopes the oxidized spiro, significantly lowers the glass transition temperature of the spiro-HTL, and can even induce the degradation of the underlying perovskite to PbI_2. Nevertheless, given its ability to produce superior film morphology and significantly enhance the HTL's conductivity, a ratio *t*BP:THF = 1:1 was determined as an optimized co-additive in our final spiro solution (**Fig. 3**).

Furthermore, while *t*BP-free and LiTFSI-free literature has been reported, as mentioned by the reviewer (e.g., TBMPTFSI in doi.org/10.1126/science.abo2757), it relies on the use of strong chemical oxidants for effective doping. This approach can introduce an excess of radicals and often involves high-cost materials. As shown in **Table R1** and **Table S15**, our LODT method has a significant cost advantage. Moreover, we have demonstrated its applicability to large-area blade-coating and its compatibility with inorganic perovskite systems, highlighting the potential practical advantages of the LODT-HTL.

Table R1. Cost assessment for the TBMPTFSI strategy. The cost analysis is based on publicly available prices for the precursor materials from major commercial chemical suppliers (Tokyo Chemical Industry Co., and Sigma-Aldrich).

Material	Amount	Price (USD/mol)
spiro	1 mol	199505
spiroTFSI2	14% mol	366960
TBMPTFSI	20% mol	24085
AgTFSI	60% mol	59008
Iodomethane	120% mol	88
*t*BP	20% mol	1884
Total price: 75460~68538 USD/mol = 62~65 USD/g		

Table S15. Cost assessment for the LODT-HTL strategy. The cost analysis is based on publicly available prices for the precursor materials from major commercial chemical suppliers (Tokyo Chemical Industry Co., and Sigma-Aldrich).

Material	Amount	Price (USD/mol)
spiro-OMeTAD	1 mol	199505
NH_4TFSI	15% mol	283
OATFSI	1% mol	361
HTFSI	16% mol	281
NH_4OH	15% mol	2
OA	1%mol	80
*t*BP+THF	10% mol	1914
Total price: 2645 USD/mol or 2 USD/g (If all additives are 100% mol)		

3#4 Most of the characterizations are done on single-component NH4TFSI spiro. But then the authors switched to using a dual-component OATFSI and NH4TFSI spiro to fabricate the devices. Does OATFSI change the spiro properties? If so, the characterizations results (e.g. oxidation process, band alignment shifts, conductivity, XPS) are not accurate anymore.

Thank you for raising the above question, which was also raised in Comment #6 from Reviewer #2 (**Response letter** Page 36). We are very sorry that our original manuscript omitted the detailed characterization of the final co-doped system using both OATFSI and NH_4TFSI. We have incorporated the missing information on Page 14, lines 368-377 of the revised manuscript:

Furthermore, we found that OATFSI functions effectively as a dopant in the LODT-HTL (**Fig. S54**) and as a co-dopant with NH_4TFSI (**Fig. 5a**), yielding a high conductivity of 3.625×10^{-3} S/cm (**Fig. S55**). DAS analysis showed that the addition of OATFSI enhanced photo-excitation process of HTL, reducing the time from 29.6 ps to 21.3 ps corresponding to the NH_4TFSI only HTL (**Fig. S56, Fig. S10**). The improvement benefits hole extraction at the device interface compared with LiTFSI-spiro as confirmed by TRPL (**Fig. 5b, Fig. S40, Table S6**). However, its ionic liquid properties can lower the T_g of HTL (72.6 °C), compromising its thermal stability (**Fig. S57**). By choosing a minimal amount of OATFSI (1% mol to spiro), maintain a T_g of 90 °C while still improving conductivity (**Fig. S55**).

In summary, our initial motivation for adding OATFSI was to leverage its acidity for further oxidizing the spiro system and to use its properties as an ionic liquid to potentially reduce the need for *t*BP. However, we found that adding OATFSI introduced some adverse effects, such as inducing a lower T_g. To counteract this, we optimized its concentration to a minimal amount (1 mol%) to ensure the final HTL maintained a high T_g of 90 °C. We also discovered that OATFSI provided benefits similar to *t*BP, such as enhancing the HTL conductivity. Furthermore, time-resolved photoluminescence (TRPL) measurements revealed that it improves hole extraction at the perovskite/HTL interface (**Fig. 5b**). This indicates that the amount of OATFSI must be carefully controlled. We ultimately chose a 1 mol% concentration primarily out of consideration for the film's thermal stability. We have confirmed that incorporating this amount of OATFSI into the final HTL does not negatively affect the spiro-HTL energy level alignment (**Fig. S37**). Finally, our results show that using OATFSI, either alone or as a co-dopant, produces good photo-response under illumination (**Fig. 5a, Fig. S54)**, suggesting a doping mechanism similar to NH_4TFSI.

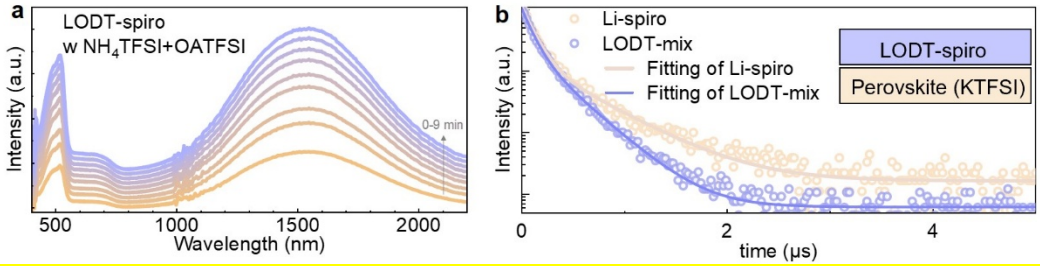

Fig. 5a,b. a, Absorption spectra evolution of the LODT-spiro solution co-doped with NH_4TFSI and OATFSI, showing increased absorbance under continuous white LED illumination within 9 min. The curve was acquired every minute. **b**, TRPL decay for perovskite films covered by a conventional LiTFSI-spiro HTL and the optimized LODT-HTL co-doped with NH_4TFSI and OATFSI.

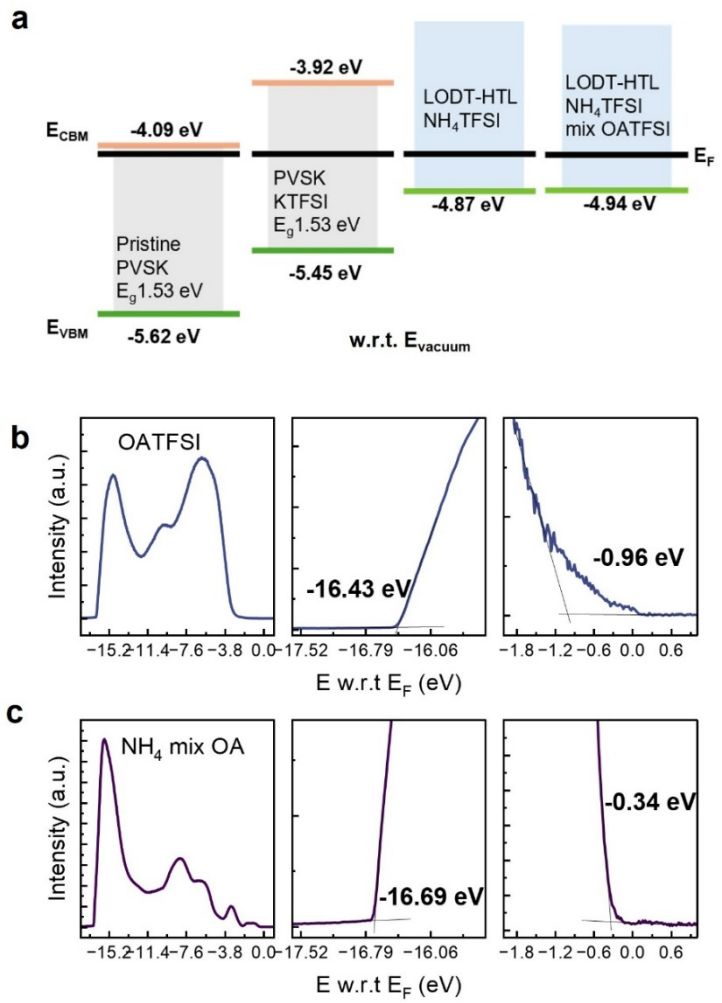

Fig. S37. Energy levels of perovskites and HTLs. a, illustration of energy level alignments between perovskites and HTLs. From left to right: pristine perovskite, KTFSI added PVSK, LODT-HTL with NH_4TFSI, and LODT-HTL co-doped with OATFSI (1% mol to spiro); E_{VBM} are collected from UPS and E_{CBM} are obtained by LEIPS, with the values represented with respect to the vacuum level (w.r.t. E_{vacuum}). UPS of **b,** LODT-HTL with OATFSI only and **c,** co-doped with NH_4TFSI and OATFSI in LODT-HTL with respect to Fermi level, E_F (w.r.t. E_F).

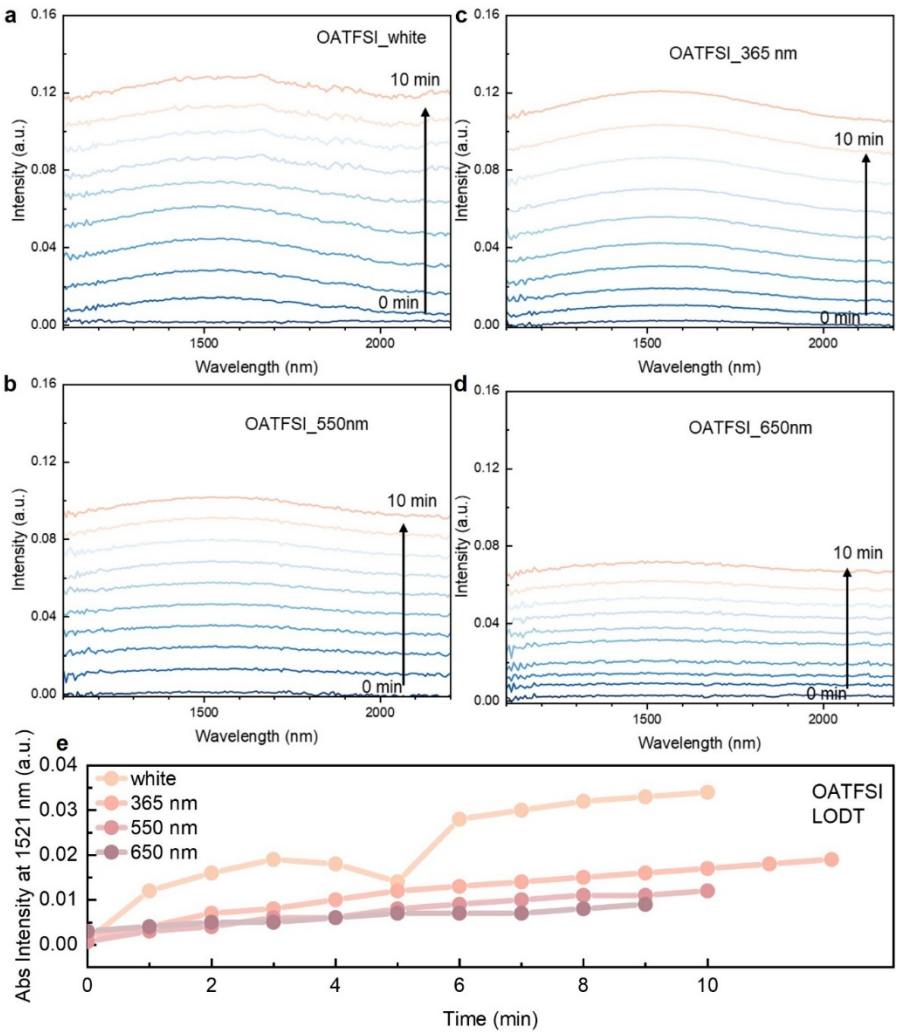

Fig. S54. Wavelength-dependent absorbance changes of spiro doped OATFSI. Time-resolved UV-Vis-NIR absorption spectra of spiro solution doped exclusively with OATFSI, measured under illumination with monochromatic light at various wavelengths of **a,** white, **b,** 365 nm, **c,** 550 nm and **d,** 650 nm. **e,** Absorbance intensity changes at 1521 nm under different light illumination for OATFSI LODT spiro solution.

Finally, we would like to once again express our sincere gratitude for your valuable questions and suggestions regarding our work. In particular, your comments on the novelty of our study and its comparison to inverted-structure devices prompted us to re-evaluate our contributions in the context of prior research. We believe our work now provides new insights for similar studies on spiro-OMeTAD doping. Specifically, we have developed a deeper and more practical understanding of the mechanism of using proton-donating dopants like ATFSI, combined with light energy, to promote spiro oxidation, including crucial details on the required illumination conditions. Furthermore, the operational stability tests

of our devices at elevated temperatures have demonstrated the advantages of this comprehensive strategy for fabricating stable, efficient, large-area perovskite modules.

Response to Reviewer #4

I co-reviewed this manuscript with one of the reviewers who provided the listed reports. This is part of the Nature Communications initiative to facilitate training in peer review and to provide appropriate recognition for Early Career Researchers who co-review manuscripts.

Reply:

Thank you for co-reviewing the manuscript and contributing to the improvement of its quality.

References:

[17] Ren, G. H., Han, W. B., Deng, Y. Y. et al. Strategies of Modifying spiro-OMeTAD Materials for Perovskite Solar Cells: A Review. Journal of Materials Chemistry A (2021) 9, 4589-4625 https://doi.org:10.1039/d0ta11564a

[18] Schloemer, T. H., Christians, J. A., Luther, J. M. & Sellinger, A. Doping Strategies for Small Molecule Organic Hole-Transport Materials: Impacts on Perovskite Solar Cell Performance and Stability. Chemical Science (2019) 10, 1904-1935 https://doi.org:10.1039/c8sc05284k

[19] Lamberti, F., Gatti, T., Cescon, E. et al. Evidence of spiro-OMeTAD De-Doping by *tert*-Butylpyridine Additive in Hole-Transporting Layers for Perovskite Solar Cells. Chem (2019) 5, 1806-1817 https://doi.org:10.1016/j.chempr.2019.04.003

[23] Abate, A., Hollman, D. J., Teuscher, J. et al. Protic Ionic Liquids as P-Dopant for Organic Hole Transporting Materials and Their Application in High Efficiency Hybrid Solar Cells. Journal of the American Chemical Society (2013) 135, 13538-13548 https://doi.org:10.1021/ja406230f

[26] Zhao, J., Cao, J., Dong, J. et al. Impact of Lithium Dopants in Hole-Transporting Layers on Perovskite Solar Cell Stability under Day–Night Cycling. Nature Energy 2025 (2025-09-01) https://doi.org:10.1038/s41560-025-01856-z

[28] Dong, Y. Y., Rombach, F. M., Min, G. H. et al. Dopant-Induced Interactions in spiro-OMeTAD: Advancing Hole Transport for Perovskite Solar Cells. Materials Science & Engineering R: Reports (2025) 162, 100875 https://doi.org:10.1016/j.mser.2024.100875

[35] Rombach, F. M., Haque, S. A. & Macdonald, T. J. Lessons Learned from spiro-OMeTAD and PTAA in Perovskite Solar Cells. Energy & Environmental Science (2021) 14, 5161-5190 https://doi.org:10.1039/d1ee02095a

[36] Kim, S. G., Fish, G. C., Socie, E. et al. Photo-Doping of spiro-OMeTAD for Highly Stable and Efficient Perovskite Solar Cells. Joule (2024) 8, 1707-1722 https://doi.org:10.1016/j.joule.2024.03.012

[37] Shin, Y. S., Song, J. W., Lee, D. G. et al. De-Doping Engineering for Efficient and Heat-Stable Perovskite Solar Cells. Joule (2025) 9, 2542-4351 https://doi.org:10.1016/j.joule.2024.10.011

[38] Streitwieser, A. & Kim, Y.-J. Ion Pair Basicity of Some Amines in THF: Implications for Ion Pair Acidity Scales1. Journal of the American Chemical Society (2000) 122, 11783–11786 https://doi.org:10.1021/ja001701

[39] Goel, M., Siegert, M., Krauss, G. et al. Homo-Homo Electron Transfer: An Elegant Strategy for P-Type Doping of Polymer Semiconductors toward Thermoelectric Applications. Advanced Materials (2020) 32, 2003596 https://doi.org:10.1002/adma.202003596

[40] Fantacci, S., De Angelis, F., Nazeeruddin, M. K. & Grätzel, M. Electronic and Optical Properties of the Spiro-OMeTAD Hole Conductor in Its Neutral and Oxidized Forms: A DFT/TDDFT Investigation. Journal of Physical Chemistry C (2011) 115, 23126-23133 https://doi.org:10.1021/jp207968b

[43] Liu, C., Sun, X., Yang, Y. et al. Retarding Solid-State Reactions Enable Efficient and Stable All-Inorganic Perovskite Solar Cells and Modules. Science Advances (2023) 9, eadg0087 https://doi.org:10.1126/sciadv.adg0087

[44] Gao, X. X., Ding, B., Kanda, H. et al. Engineering Long-Term Stability into Perovskite Solar Cells Via Application of a Multi-Functional TFSI-Based Ionic Liquid. Cell Reports Physical Science (2021) 2, 2666-3864 https://doi.org:10.1016/j.xcrp.2021.100475

[45] Huo, X. M., Mariotti, S., Li, Y. Y. et al. Unraveling the Relationship between the Phenethylammonium-Induced 2D Phase on the Perovskite Surface and Inverted Wide Bandgap Perovskite Solar Cell Performance. Energy & Environmental Science (2024) 17, 8658-8669 https://doi.org:10.1039/d4ee02133a

[S2] Fantacci, S., De Angelis, F., Nazeeruddin, M. K. & Grätzel, M. Electronic and Optical Properties of the Spiro-Meotad Hole Conductor in Its Neutral and Oxidized Forms: A DFT/TDDFT Investigation. Journal of Physical Chemistry C (2011) 115, 23126-23133 https://doi.org:10.1021/jp207968b

[S4] Hawash, Z., Ono, L. K., Raga, S. R., Lee, M. V. & Qi, Y. B. Air-Exposure Induced Dopant Redistribution and Energy Level Shifts in Spin-Coated Spiro-Meotad Films. Chemistry of Materials (2015) 27, 562-569 https://doi.org:10.1021/cm504022q
[S5] Lee, J. H., Kim, T., Song, S. et al. Enhanced Band-Filling Effect in Halide Perovskites Via Hydrophobic Conductive Linkers. Cell Reports Physical Science (2022) 3, 2666-3864 https://doi.org:10.1016/j.xcrp.2022.100800
[S6] Chen, W., Pham, N. D., Wang, H., Jia, B. & Wen, X. Spectroscopic Insight into Efficient and Stable Hole Transfer at the Perovskite/spiro-OMeTAD Interface with Alternative Additives. ACS Applied Materials & Interfaces (2021) 13, 5752-5761 https://doi.org:10.1021/acsami.0c19111
[S11] Zhao, J. Z., Cao, J. P., Dong, J. J. et al. Impact of Lithium Dopants in Hole-Transporting Layers on Perovskite Solar Cell Stability under Day-Night Cycling. Nature Energy (2025), 1-11 https://doi.org:10.1038/s41560-025-01856-z
[S12] Cao, F., Zhu, Z., Zhang, C. et al. Synergistic Ionic Liquid in Hole Transport Layers for Highly Stable and Efficient Perovskite Solar Cells. Small (2023) 19, e2207784 https://doi.org:10.1002/smll.202207784
[S13] Jung, S. K., Park, K., Lee, J. H. et al. Exploiting an Interfacial Reaction in Perovskite Solar Cells: Quaternary Alkylammonium Ionic Salt Dopants for spiro-OMeTAD. Advanced Energy Materials (2025) 15 https://doi.org:10.1002/aenm.202402144
[S14] Nishimura, N., Kanda, H. & Murakami, T. N. Direct Ion-Exchange Method for Preparing a Solution Allowing Spontaneous Perovskite Passivation via Hole Transport Material Deposition. ACS Applied Energy Materials (2024) 7, 7687-7692 https://doi.org:10.1021/acsaem.4c01314